Scientific report; WR 99 - 02

KNMI

Turbulent air flow over sea waves: simplified model for applications

V.N. Kudryavtsev, V.K. Makin and J.F. Meirink

De Bilt, 1999

Scientific report = wetenschappelijk rapport; WR 99 - 02

De Bilt, 1999

PO Box 201
3730 AE De Bilt
Wilhelminalaan 10
De Bilt
The Netherlands
Telephone + 31(0)30-220 69 11
Telefax + 31 (0)30-221 04 07

Author: V.N. Kudryavtsev, V.K. Makin and J.F. Meirink

UDC: 551.466.1
551.526.63
551.551.8

ISSN: 0169-1651

ISBN: 90-369-2158-9

Turbulent air flow over sea waves: simplified model for applications

V.N. Kudryavtsev[1], V.K. Makin[2] and J.F. Meirink[2]

[1] *Marine Hydrophysical Institute*
Sevastopol, Ukraine

[2] *Royal Netherlands Meteorological Institute (KNMI)*
De Bilt, The Netherlands

Contents

Abstract 2

1 Introduction 3

2 Model equations 5
- 2.1 Wave-induced variations of wind velocity . . . 5
- 2.2 Inner and outer region . . . 7
  - 2.2.1 The role of the critical layer . . . 8

3 Solution of equations 9
- 3.1 The outer region . . . 9
  - 3.1.1 The inviscid air flow . . . 10
  - 3.1.2 The outer region in the turbulent air flow . . . 11
- 3.2 The inner region . . . 12
  - 3.2.1 Reynolds stresses . . . 12
  - 3.2.2 Vorticity equation in the IR . . . 13
  - 3.2.3 Horizontal velocity . . . 14
  - 3.2.4 Patching the ISL and SSL solutions . . . 16
  - 3.2.5 Vertical velocity . . . 16
  - 3.2.6 Shear stress variations . . . 17
- 3.3 Energy transfer from wind to wave . . . 18

4 Results 19
- 4.1 Wind velocity and shear stress profiles . . . 19
- 4.2 Comparison with measurements . . . 21
- 4.3 Comparison of predicted growth rate with WBL-model and Miles' theory . 22

5 Discussion and conclusions 23

Acknowledgements 24

A Appendices 25
- A.1 Langer's method . . . 25
- A.2 Airy functions . . . 26
- A.3 Numerical solution . . . 26

References 28

Figures 29

Abstract

A simplified model of the air flow over surface water waves propagating at arbitrary phase velocity (as compared to the wind speed, e.g. at 10 m) and direction (relative to the wind direction) is presented. The air flow is divided into an outer (OR) and an inner (IR) regions. In the OR the wave-induced motions experience inviscid undulation, while in the IR they are strongly affected by turbulent shear stresses. Introduction of the OR and the IR allows a considerable simplification in the description of the air flow above waves.

The critical height (the height where the wind speed and the wave phase velocity are equal) is for most cases located inside the IR. Hence, its singular behaviour is strongly suppressed by turbulent stresses. This fact allows a simple description of the wind velocities in the OR, which is based on the approximate solution of the Rayleigh equation suggested by Miles (1957).

The description of the IR is based on the solution of the vorticity equation accounting for the turbulent diffusion. The turbulent shear stress is parameterised via the eddy viscosity coefficient adopting the mixing length closure scheme. Exponential damping of the shear stress variations with height towards the OR is introduced, which leads to further simplification. This damping describes phenomenologically the basic feature of the wave boundary layer: rapid distortion of turbulence in the OR.

The model is reduced to a set of explicit analytical formulas which describe the wind velocities and shear stresses in the boundary layer above the waves. Results of the simplified model (velocities and shear stress profiles, the growth rate) are in reasonable agreement with those obtained by a two-dimensional numerical model based on the second-order closure scheme. This fact is encouraging, and has an important consequence: the description of the air flow dynamics over waves is not sensitive to the details of the closure schemes. It is only important to provide the vertical damping of variations in turbulence characteristics on a scale comparable with the IR height.

The simplified model is compared with data of the laboratory experiment of Hsu and Hsu (1983), and reasonable agreement in velocity and shear stress distributions is found.

1 Introduction

The physical phenomena which occur on the air-water interface, are defined or strongly influenced by the air flow dynamics over the water surface. Exchange of momentum, heat, moisture and gases between the atmosphere and the ocean is determined to a large extent by the wind-wave interactions. A significant part of the momentum flux at the sea surface is formed directly by wind waves. As breaking waves eject spray into the atmosphere, they could enhance the exchange of heat and moisture. To account for this process the vertical transport and spreading of spray, defined by the air flow above waves, should be known. Short wind waves, the key issue in remote sensing application, are formed and modulated by the wind. To understand and parameterise the processes which occur at the sea surface and in the adjacent part of the air boundary layer, an explicit description of the air flow over waves is needed.

Starting from Miles (1957) numerous studies have been dedicated to the problem (see, e.g., a recent review of Belcher and Hunt, 1998). Recently, it became clear that the modulations of the Reynolds stresses close to the wave surface are responsible for the peculiarities of the wind-wave interaction. Belcher and Hunt (1993) introduced the sheltering mechanism of wave growth. They distinguish two main layers above the waves: the inner and the outer layer. In the inner layer, a very thin region adjacent to the surface, the wave-induced turbulence is in local equilibrium with the local wind shear. In contrast, in the outer region the turbulent stresses correlated with the wave surface are suppressed due to rapid distortion effects, so that there the dynamics corresponds to inviscid flow. The action of the Reynolds stresses in the inner region causes a thickening of the stream lines on the forward slope of wave. The inner region is thus asymmetric, leading to a pressure asymmetry in the outer region which results in wave growth. The introduction of the inner and outer region in the description of the turbulent boundary layer above waves is very productive and helps considerably to simplify the analysis of the air flow dynamics above waves. Belcher and Hunt (1993) found an analytical solution for the case of slow waves. Harris et al. (1996) developed an eddy viscosity model in which the turbulent stresses in the inner region are parameterised by using the eddy viscosity derived from the balance between the turbulent kinetic energy (TKE) production and its dissipation. In the outer region the eddy viscosity coefficient is damped exponentially, and the turbulent stresses vanish.

We present here a simplified model of the wave boundary layer (SWBL), which can be used as a simple module in a variety of studies where the detailed structure of the air flow above waves is required. As an example we mention the calculation of stresses in the model of short waves modulation by long waves (Kudryavtsev et al, 1997), or the calculation of the wave-induced velocity field to study the distribution of sea spray. The SWBL model can also be useful to support experimental studies, both in the stage of preparation and measurements, when a quick decision to correct/extend measurements is needed and the use of expensive large numerical models of the boundary layer is not feasible. The SWBL model is designed to describe the air flow above fast and slowly moving waves (as compared to the wind velocity), and propagating at arbitrary angle to the wind direction.

The main conceptional simplification of the problem is based on the division of the turbulent boundary layer into two parts: the outer and the inner region, after Belcher and Hunt (1993). In the outer region (OR) the wave-induced motions experience undulations typical for inviscid flow. The description of the outer region is considerably simplified by the use of the approximate solution of the Rayleigh equation for the vertical velocity suggested by Miles (1957) and Lighthill (1957). The amplitude of the vertical velocity is proportional to the mean velocity profile, and decays exponentially with height. The horizontal velocity is found with the same accuracy from the vorticity conservation equation, where the vertical velocity is known.

In the inner region (IR) the dynamics of wave-induced motions is affected strongly by turbulent stresses. Towards the outer region stresses are damped exponentially. Unlike Harris et al. (1996), who introduced damping of the eddy viscosity coefficient, we introduce damping directly on stresses. The local eddy viscosity closure scheme is used to parameterise those stresses. The eddy viscosity coefficient is obtained from the balance between the turbulent kinetic energy production and its dissipation, where the dissipation is expressed in terms of the mixing length. The description of the inner region is based on the solution of the vorticity equation. The method of Langer (1934) is used to solve the equation, taking into account the existence of the critical layer. The solution in the inner layer is patched to the outer layer solution, and the explicit formulas for the velocity and stresses are obtained.

The solution of the simplified model is compared with the results of the 2 dimensional (2D) numerical wave boundary layer (WBL) model (Mastenbroek et al., 1996), based on a second-order Reynolds stress closure scheme. A good quantitative and qualitative agreement, both in velocity and stress distribution, and for fast and slow waves is shown. The estimate of the growth rate parameter obtained by the SWBL model is consistent with the 2D WBL model.

The results of the SWBL model are compared with data of Hsu and Hsu (1983) obtained in laboratory conditions. The comparison is encouraging: the simplified model reproduces well the measurements of velocity and shear stress fields above waves. The main model assumption (division of the air flow into an outer and inner region) is supported by the measurements.

2 Model equations

2.1 Wave-induced variations of wind velocity

A fully developed turbulent air flow over a monochromatic surface wave travelling on the (x_1, x_2) plane along the x_1-axis with the phase speed c is considered. The air flow moves at an angle θ to the x_1-axis, and all the air flow variables are uniform along the x_2-axis. The surface is described by

$$\eta = \eta_o(kx_1 - \omega t), \tag{1}$$

where k and ω are the wavenumber and the frequency of the surface wave. In a frame that moves with the phase speed of the wave the equations governing the steady air flow are

$$\begin{aligned}
u\frac{\partial u}{\partial x_1} + w\frac{\partial u}{\partial x_3} &= -\frac{\partial}{\partial x_1}(p - \tau_{33}) + \frac{\partial}{\partial x_3}\tau_{13} + \frac{\partial}{\partial x_1}(\tau_{11} - \tau_{33}), &(2)\\
u\frac{\partial w}{\partial x_1} + w\frac{\partial w}{\partial x_3} &= -\frac{\partial}{\partial x_3}(p - \tau_{33}) + \frac{\partial}{\partial x_1}\tau_{13}, &(3)\\
\frac{\partial}{\partial x_1}u + \frac{\partial}{\partial x_3}w &= 0, &(4)
\end{aligned}$$

where p is the pressure, τ is the Reynolds shear stress, τ_{11} and τ_{33} are the Reynolds normal stresses.

We use a wave-following coordinate system

$$\begin{aligned}
x &= x_1,\\
z &= x_3 - \eta(x_1, x_3),
\end{aligned} \tag{5}$$

where $\eta(x_1, x_3) = \eta_o(x_1)\exp(-kx_3)$. Equations (2)-(4) then take the form

$$\begin{aligned}
u(\frac{\partial}{\partial x} - \eta_1\frac{\partial}{\partial z})u + w(1-\eta_3)\frac{\partial}{\partial z}u &= -(\frac{\partial}{\partial x} - \eta_1\frac{\partial}{\partial z})P + (1-\eta_3)\frac{\partial}{\partial z}\tau_{13}\\
&\quad +(\frac{\partial}{\partial x} - \eta_1\frac{\partial}{\partial z})(\tau_{11} - \tau_{33}), &(6)\\
u(\frac{\partial}{\partial x} - \eta_1\frac{\partial}{\partial z})w + w(1-\eta_3)\frac{\partial}{\partial z}w &= -(1-\eta_3)\frac{\partial}{\partial z}P + (\frac{\partial}{\partial x} - \eta_1\frac{\partial}{\partial z})\tau_{13}, &(7)\\
(\frac{\partial}{\partial x} - \eta_1\frac{\partial}{\partial z})u + (1-\eta_3)\frac{\partial}{\partial z}w &= 0, &(8)
\end{aligned}$$

where $P = p - \tau_{33}$, and $\eta_1 = \partial\eta/\partial x_1$, $\eta_3 = \partial\eta/\partial x_3$. The vertical transformation of the x_3-coordinate is defined so that the lines $z = \text{const}$ are related to the streamlines of the irrotational flow over the wave.

The slope of the surface wave is small, so that the air flow can be described as a sum of the basic flow and small perturbations

$$u(x, z) = U(z) + \tilde{u}(x, z),$$

$$
\begin{aligned}
v(x,z) &= V(z), \\
w(x,z) &= \tilde{w}(x,z), \\
P(x,z) &= \overline{P}(z) + \tilde{P}(x,z), \\
\tau_{ij}(x,z) &= \overline{\tau}_{ij}(z) + \tilde{\tau}_{ij}(x,z).
\end{aligned} \tag{9}
$$

Here the wind velocity components U, V and the variables marked by bars are related to the basic flow averaged over the x-coordinate, while tildes refer to the perturbed flow. For a small air flow perturbation equations (6) - (8) can be linearized (hereafter the tilde over the perturbed variables is omitted) so that

$$
U\frac{\partial u}{\partial x} + (w - \eta_1 U)\frac{\partial U}{\partial z} = -\frac{\partial P}{\partial x} + \frac{\partial \tau_{13}}{\partial z} + \frac{\partial}{\partial x}(\tau_{11} - \tau_{33}), \tag{10}
$$

$$
U\frac{\partial w}{\partial x} = -\frac{\partial P}{\partial z} + \frac{\partial \tau_{13}}{\partial x}, \tag{11}
$$

$$
\frac{\partial u}{\partial x} - \frac{\partial}{\partial z}(w - \eta_1 U) = -\eta_{13} U, \tag{12}
$$

where $\eta_{13} = \partial^2 \eta / \partial x_1 \partial x_3$. The mean wind velocity profile is assumed to vary logarithmically

$$
\begin{aligned}
U(z) &= (\overline{u}_*/\kappa)\ln(z/z_0)\cos\theta - c \\
&= (\overline{u}_*/\kappa)\ln(z/z_c)\cos\theta.
\end{aligned} \tag{13}
$$

Here κ is the Von Karman constant, z_0 is the roughness parameter, $\overline{u}_*$ is the friction velocity in the basic flow, and z_c is the critical height defined as

$$
z_c = z_0 \exp\left(\frac{\kappa c}{\overline{u}_* \cos\theta}\right). \tag{14}
$$

The roughness parameter is taken as the sum of the Charnock relation and the viscous roughness scale to account for low winds

$$
z_0 = 0.014 u_*^2/g + 0.11 \nu_a / u_*, \tag{15}
$$

where ν_a is the kinematic viscosity of the air.

The air flow perturbations can be now calculated from (10)-(12) with the boundary conditions:

$$
u, w, P, \tau_{ij} \to 0, \tag{16}
$$

if $z \to \infty$, and

$$
u = u_s, \tag{17}
$$

$$
w = -c\partial\eta_0/\partial x \tag{18}
$$

at $z = z_0$, where u_s is the horizontal component of the surface wave orbital velocity.

The vorticity equation for the perturbed flow results from equations (10)-(12) by elimination of P

$$U\frac{\partial\Omega}{\partial x} + (w - \eta_1 U)U'' - \eta_{13}UU' = (\frac{\partial^2}{\partial z^2} - \frac{\partial^2}{\partial x^2})\tau_{13} + \frac{\partial^2}{\partial x \partial z}(\tau_{11} - \tau_{33}), \tag{19}$$

where $\Omega = \partial u/\partial z - \partial w/\partial x$ is the vorticity, $U' = \partial U/\partial z$, and $U'' = \partial^2 U/\partial z^2$. The vorticity equation can be rewritten as the Rayleigh equation for the vertical velocity using the continuity equation (12)

$$U(\frac{\partial^2 w}{\partial z^2} + \frac{\partial^2 w}{\partial x^2}) - wU'' = -(\frac{\partial^2}{\partial z^2} - \frac{\partial^2}{\partial x^2})\tau_{13} - \frac{\partial^2}{\partial x \partial z}(\tau_{11} - \tau_{33}). \tag{20}$$

Equation (19) can be solved after the Reynolds stresses are expressed in terms of the independent variables, i.e. the turbulence closure scheme has to be introduced.

2.2 Inner and outer region

Belcher and Hunt (1993) developed scaling arguments to describe how turbulence in the air flow is affected by a surface wave. They introduced two main time scales. The advection time scale, $T_D \sim k^{-1}/|U(z)|$, characterizes the time for turbulent eddies to be advected and distorted by the mean flow over the wave. The eddy turnover time scale, $T_L \sim \kappa z/u_*$, characterizes the time for eddies to be dissipated, when the turbulence is in equilibrium with the local wind shear. The height at which these scales are comparable $T_D \sim T_L$ is defined as the height of the inner region l. Belcher and Hunt (1993) give an estimate

$$kl = 2\kappa u_*/|U(l)|. \tag{21}$$

In a case of very fast waves the estimate is $kl = 2\kappa u_*/c$. In the inner region $z < l$ the turbulence tends to a local equilibrium with the local wind shear. In the outer region $z > l$ turbulent eddies are advected too fast to be correlated with the local wind shear. The turbulent stresses are smeared out, i.e. they are not correlated with the surface wave, and the wave-induced air flow in the OR becomes inviscid.

The inner region has an important physical meaning. It represents the region in the boundary layer above the wave where disturbances of turbulent stresses (and other characteristics of turbulence), caused by the interaction of the air flow with the surface, are located. Experimental evidence of the existence of the IR above waves was presented by Mastenbroek et al. (1996).

The height of the IR is the key parameter in the present model. It is shown as a function of the inverse wave age parameter U_k/c (U_k is the wind speed at $z = k^{-1}$) in Figure 1. For a given wind, the IR height increases with increasing phase speed and reaches its maximal values in the vicinity of $U_k/c \sim 1$. This corresponds to waves at the peak of the wave spectrum of a fully developed sea. For faster waves the IR height decreases again.

The subdivision of the boundary layer above waves into an inner and an outer region considerably simplifies the parameterization of the Reynolds stresses. In the outer region

the turbulent stresses are simply neglected, and the air flow experiences inviscid undulation. In the inner region simple local eddy-viscosity schemes can be used. Here the air flow is strongly affected by wave-induced variations of turbulent stresses. We thus introduce a two layer air flow model. The boundary between the two layers is specified at height $h = nl$, where n is a constant of order 1. At height $z = h$ the wind velocity and its vertical gradient are continuous.

2.2.1 The role of the critical layer

The critical layer plays a crucial role in quasi-laminar models of the air flow above waves (Miles, 1957). This type of models assumes that the turbulent stresses can be neglected. In the terminology of the rapid distortion theory above waves this assumption is only valid when the height of the critical layer is situated in the outer region (Belcher and Hunt, 1998). The height z_c of the critical layer, defined by the condition $U(z_c) = 0$, equation (14), is shown in Figure 1. In the range of $U_k/c > 1$ the critical layer is located inside the inner region, so that the turbulent stresses should influence the dynamics of the critical layer.

Miles (1959) indicated that viscous effects become important and break down the assumption of the quasi-laminar model when the viscous scale of the critical layer

$$\delta_c = (\nu_a \kappa z_c / \overline{u}_* k)^{1/3} \tag{22}$$

is of order z_c or more, i.e. $\delta_c \geq z_c$.

If the critical layer is situated within the inner layer of the turbulent flow the eddy-viscosity takes the role of the molecular viscosity. The estimate of the height δ_c in this case can be made by replacing the viscosity ν_a in equation (22) by the eddy viscosity $K = 2\kappa \overline{u}_* z$ at $z = z_c$ (see equation (44) below). Then the estimate (22) becomes

$$\delta_c = (2\kappa^2 z_c^2 / k)^{1/3} \tag{23}$$

and the condition $\delta_c \geq z_c$ is equivalent to

$$k z_c \leq 2\kappa^2.$$

From Figure 1 it follows that both conditions $z_c < l$ and $k z_c \leq 2\kappa^2$ are satisfied in the range of $U_k/c > 1$. It means that in this range turbulence dominates the dynamics of the air flow in the vicinity of the critical height. Hence, the applicability of quasi-laminar models in the description of the air flow dynamics is restricted to a very narrow range of the parameter U_k/c around $U_k/c \simeq 1$.

3 Solution of equations

Any flow variable in the air Y experiences a small variation $\widetilde{Y}$ in the presence of waves. The wave steepness ak (a is the wave amplitude) is assumed to be small, and the variation can be expanded in powers of ak, namely

$$\widetilde{Y}(x,z) = \langle Y \rangle \, (akY^{(1)}(x,z) + O(ak^2)), \tag{24}$$

where $\langle Y \rangle$ is a scaling argument. The second small parameter of the problem is the dimensionless scale of the IR kl. As the variable $Y^{(1)}$ could depend on kl, we expand $Y^{(1)}(x,z)$ in powers of kl

$$Y^{(1)}(x,z) = Y_0(x,z) + klY_1(x,z) + O(k^2l^2). \tag{25}$$

To normalize variations in the air flow parameters, u_*/κ is chosen as a scale for the wind velocities (including the background wind speed), and $\overline{u}_*^2$ as a scale for the Reynolds stresses and pressure.

The surface wave is introduced as the real part of

$$\eta_0(x) = ae^{ikx}. \tag{26}$$

The solution of the problem is presented in the form of normal modes

$$Y^{(1)}(x,z) = \widehat{Y}(z)e^{ikx}, \tag{27}$$

where $\widehat{Y}(z) = \widehat{Y}_r(z) + i\widehat{Y}_i(z)$ is a complex amplitude. It can be also expanded in powers of kl

$$\widehat{Y}(z) = \widehat{Y}_0(z) + kl\widehat{Y}_1(z) + ... \tag{28}$$

The real part of $\widehat{Y}(z)$ is the amplitude of the wave-induced variation in the air flow which is correlated with the wave elevation. The imaginary part of $\widehat{Y}(z)$ is the amplitude of the variation which is correlated with the wave slope. Notice that if $\widehat{Y}_i(z)$ is positive then the maximum of the wave induced variation is displaced towards the rear slope of the wave. As the surface wave is described by $a\cos(kx)$, only the real part of (27) has a physical sense.

The analysis is carried out in first-order in ak (hereafter the superscript 1 is omitted), and in zero-order in kl. This solution is called the zero-order solution). For the vertical velocity the first order kl-correction of the zero-order solution has a significant physical sense (see Section 3.2.5), and will be considered additionally.

3.1 The outer region

The turbulent stresses in the outer region are not correlated with the surface wave. Hence, the wave-induced motions in the OR should be close to that of the inviscid air flow.

3.1.1 The inviscid air flow

When the air flow experiences an inviscid undulation over the surface wave, eq.(20) is reduced to the Rayleigh equation

$$U(\frac{\partial^2 \hat{w}_0}{\partial z^2} - k^2 \hat{w}_0) - \hat{w}_0 U'' = 0, \tag{29}$$

with the boundary conditions for the vertical velocity (16), (17), and (18). This equation has been studied in details in numerous papers starting from Miles (1957).

Miles (1957) and Lighthill (1957) suggested an approximate solution of the Rayleigh equation in the form

$$\hat{w}_0(z) = \gamma U(z) \exp(-kz), \tag{30}$$

where γ is a constant of proportionality. As it was mentioned by Phillips (1966), this constant should have a different value above and below the critical height. At $z < z_c$ the constant must be $\gamma = i$ to satisfy the boundary condition (16). At $z > z_c$ the constant should differ from i due to the expected influence of the critical layer dynamics. Direct substitution of (30) in (29) shows that this solution satisfies the Rayleigh equation with the accuracy of $(kz \ln(kz/kz_c))^{-1}$ at "large" distance from the surface ($kz \sim 1$), and with the accuracy of kz close to the surface ($kz << 1$).

To check the approximate solution (30), it is compared with a numerical solution of the Rayleigh equation (29). The results of the numerical integration of the Rayleigh equation along with the approximate solution (30) for the inverse wave age parameter $U_{10}/c = 5$ and 2 are presented in Figure 2. To fit (30) to the "exact" solution the tuning constant γ is chosen as:

$$\gamma = \begin{cases} i & \text{if } z < z_c, \\ \frac{1}{2} + \frac{1}{2}i & \text{if } z > z_c. \end{cases} \tag{31}$$

This choice gives reasonable agreement between the approximate solution (30) and the numerical solution. Note that at the critical height eq.(30) gives $\hat{w}_{0r}(z_c) = 0$. However, in fact $\hat{w}_{0r}(z_c)$ is slightly positive. Its value defines the energy transfer from the shear flow to waves in the quasi-laminar theory of Miles (1957). As was proposed by Miles (1957), the magnitude of the vertical velocity at the critical height can be estimated through the approximate solution (30). Integrating eq.(11) with $\hat{w}_0$ defined by (30) from infinity to z_c, and substituting the obtained relation for the imaginary part of $\hat{P}$ into eq. (10), we obtain the following relation

$$\hat{w}_0(z_c) = Re(\gamma) \frac{\kappa k z_c}{u_*} \int_{z_c}^{\infty} U^2 e^{-kz} d(kz). \tag{32}$$

In Section 3.3 this relation for the vertical velocity at $z = z_c$ will be used to calculate the growth rate parameter in an inviscid boundary layer (Miles' theory).

The approximate solution for the horizontal velocity can be obtained (via $\hat{w}_0$ defined by (30)) either from the continuity equation (12) or from the continuity equation (4) depending on which coordinate system is used. In the regular fixed (x_1, x_3) coordinate system the approximate solution for the horizontal velocity reads

$$\hat{u}_0(x_3) = i\gamma \left[-U + k^{-1} U'\right] e^{-kx_3}. \tag{33}$$

This solution is shown in Figure 2 along with the numerical solution of the Rayleigh equation for different wave ages. The approximate description of both horizontal and vertical motions compares reasonably well with the numerical solution. We shall apply this approach for the approximate description of the outer region in the turbulent boundary layer.

3.1.2 The outer region in the turbulent air flow

As was mentioned in Section 2.2.1, the singular behaviour of the critical layer dynamics in the turbulent air flow over a surface wave must be suppressed significantly. Hence, we may suppose that the vertical velocity in the OR has to be described approximately by eq. (30) with $\gamma = i$ (to satisfy the lower boundary condition) throughout the whole wave boundary layer, i.e.

$$\widehat{w}_0(z) = iU(z)e^{-kz}. \tag{34}$$

This solution describes the basic behaviour of vertical motions in the turbulent boundary layer caused the surface wave. However, as will be shown later, this solution is correct only in zero-order. The dynamics of the Reynolds stresses inside the IR results in vertical motions which are of $kl-$order (see Belcher and Hunt (1993) in the case of slow waves).

The estimate of the horizontal velocity resulting from the continuity equation with $\widehat{w}_0$ from (34) looks reasonable if the main peculiarity in the $\widehat{u}_0$ profile is caused by the singular behaviour of the critical layer. In the case of a turbulent boundary layer this singular behaviour in $\widehat{u}_0$ must be significantly blurred, and we need a more accurate estimate of the horizontal velocity.

The estimate of $\widehat{u}_0$ via the continuity equation is not appropriate since it is derived by differentiation of the approximate solution (34). This procedure can result in a decrease in accuracy. To get the solution of $\widehat{u}_0$ with the same accuracy as $\widehat{w}_0$, we have to use the vorticity equation (20). In terms of normal modes this equation takes the form:

$$ikU(\frac{\partial \widehat{u}_0}{\partial z} - ik\widehat{w}_0) + (\widehat{w}_0 - ie^{-kz}U)U'' + ike^{-kz}UU' = 0. \tag{35}$$

Substituting the approximation (34) for $\widehat{w}_0$ into the vorticity equation, and then integrating the obtained expression for $\partial\widehat{u}_0/\partial z$ from ∞ to z (satisfying the condition $\widehat{u}_0(\infty) = 0$), we obtain the following approximate solution for the horizontal velocity:

$$\widehat{u}_0(z) = Ue^{-kz} + 2\int_z^\infty e^{-kz_1}U'dz_1. \tag{36}$$

Summarizing, the general features of the wave-induced motions in the outer region are described by eqs.(34) and (36) for the vertical and the horizontal component of the wind velocity respectively. These are the "zero-order" solutions (in the sense of expansion (25) in kl-powers). The kl-correction of the solution for $\widehat{u}_0(z)$ does not introduce new essential elements in the description of the horizontal velocity in the OR. However the kl-correction of the vertical velocity is important as $Re(\widehat{w})$ plays a dominant role in the energy transfer from wind to waves (see Sections 3.2.5 and 3.3).

3.2 The inner region

3.2.1 Reynolds stresses

In the inner region the Reynolds stresses are in equilibrium with the local gradient of the wind velocity. Consequently, they can be described by the local eddy viscosity closure scheme

$$\tau_{13} = K\left(\frac{\partial u}{\partial z} + \frac{\partial w}{\partial x}\right), \tag{37}$$

$$\tau_{23} = K\frac{\partial v}{\partial z}. \tag{38}$$

Here K is the eddy viscosity coefficient which is expressed via the square root of the turbulence kinetic energy e (TKE) and the turbulence length scale, which is proportional to the distance from the surface

$$K = \kappa z e^{1/2}. \tag{39}$$

Furthermore, the normal Reynolds stresses in the IR are proportional to the shear stress

$$\tau_{11} = -\alpha_u(\tau_{13}^2 + \tau_{23}^2)^{1/2}, \tag{40}$$

$$\tau_{33} = -\alpha_w(\tau_{13}^2 + \tau_{23}^2)^{1/2}. \tag{41}$$

The shear stress can be found from the TKE conservation equation, where local balance between TKE production by shear of the horizontal velocity component and its dissipation is assumed. In first kl-order this balance reads

$$\tau_{13}\partial u/\partial z + \tau_{23}\partial v/\partial z - e^{3/2}/\kappa z = 0. \tag{42}$$

The linearized equation (42) written in normal modes is

$$\widehat{\tau}_{13}\frac{\partial U}{\partial z} + \overline{\tau}_{13}\frac{\partial \widehat{u}}{\partial z} = \frac{3}{2}\frac{\overline{e}^{1/2}}{\kappa z}\widehat{e}. \tag{43}$$

The shear stress is derived from (37), (39), and (43):

$$\begin{aligned}\widehat{\tau}_{13} &= \widehat{K}\partial U/\partial z + \overline{K}\partial\widehat{u}/\partial z \\ &= \left(\frac{3+\cos^2\theta}{3-\cos^2\theta}\right)\kappa z\overline{u}_*\frac{\partial\widehat{u}}{\partial z}.\end{aligned} \tag{44}$$

This expression is valid well inside the IR, at $z < l$. As the height approaches the outer region, the shear stress has to attenuate. To take this effect into account, we introduce vertical damping of the shear stress. Then (44) takes the form

$$\widehat{\tau}_{13} = \kappa z\overline{u}_*\left(\frac{3+\cos^2\theta}{3-\cos^2\theta}\right)e^{-z/l}\frac{\partial\widehat{u}}{\partial z}. \tag{45}$$

At small z/l this equation reduces to (44), and at large z/l the shear stress vanishes.

Harris et al. (1996) introduced damping of the eddy viscosity to suppress stresses in the OR. The direct damping of the shear stress, proposed here, is as effective and more straightforward.

3.2.2 Vorticity equation in the IR

Let us rewrite the vorticity equation (19) in the dimensionless vertical coordinate

$$\zeta = z/l. \tag{46}$$

Taking into account relations for the shear and normal stresses (45), (40), and (41), the vorticity equation (19) in terms of normal modes takes the form

$$\begin{aligned} & iU(\frac{\partial \widehat{u}}{\partial \zeta} - ikl\widehat{w}) + (kl)^{-1}(\widehat{w} - ie^{-kl\zeta}U)U''_{\zeta\zeta} + ie^{-kl\zeta}UU'_{\zeta} \\ = \; & \frac{(3+\cos^2\theta)}{2(3-\cos^2\theta)}\frac{\kappa\,|U_l|}{\overline{u}_*}\left[\frac{\partial^2}{\partial\zeta^2} + (kl)^2 - ikl\cos\theta(\alpha_u - \alpha_w)\frac{\partial}{\partial\zeta}\right]\left(\zeta e^{-\zeta}\frac{\partial\widehat{u}}{\partial\zeta}\right). \end{aligned} \tag{47}$$

The continuity equation (12) reads

$$ikl\widehat{u} + \frac{\partial\widehat{w}}{\partial\zeta} - ie^{-kl\zeta}U'_{\zeta} = 0, \tag{48}$$

where $U'_{\zeta} = \partial U(\zeta)/\partial\zeta$ and $U''_{\zeta\zeta} = \partial^2 U(\zeta)/\partial\zeta^2$.

It was shown (see Figure 1) that the height of the IR kl is small except in a narrow range in the vicinity of $U_{10}/c \sim 1.2$. Thus, outside this narrow range the terms of kl-order can be neglected in equation (47) and it takes the form

$$\frac{(3+\cos^2\theta)}{2(3-\cos^2\theta)}\frac{\partial^2}{\partial\zeta^2}\left(\zeta e^{-\zeta}\frac{\partial\widehat{u_0}}{\partial\zeta}\right) - i\frac{\overline{u}_* U}{\kappa\,|U_l|}\frac{\partial\widehat{u}_0}{\partial\zeta} = \Gamma(\zeta), \tag{49}$$

where the function $\Gamma(\zeta)$ is

$$\begin{aligned} \Gamma(\zeta) &= \frac{\overline{u}_*}{\kappa\,|U_l|}\left[\frac{(\widehat{w} - ie^{-kl\zeta}U)U''_{\zeta\zeta}}{kl} + ie^{-kl\zeta}UU'_{\zeta}\right] \\ &= \frac{\overline{u}_*}{\kappa\,|U_l|}\left[\widehat{w}_1 U''_{\zeta\zeta} + ie^{-kl\zeta}UU'_{\zeta}\right]. \end{aligned} \tag{50}$$

To obtain the second equality the expansion (28) in kl-power series for the vertical velocity is used, so that $\widehat{w}_0$ is defined by (34) and $\widehat{w}_1$ is the kl-order correction. The term Γ describes the source of vorticity caused by vertical motions in the shear flow.

The kl-order correction of the vertical velocity can be found from the continuity equation (48) if the zero-order solution for $\widehat{u}$ is known

$$\widehat{w}_1(\zeta) = -ikl\int_{\zeta_0}^{\zeta}(\widehat{u}_0 - Ue^{-kl\zeta_1})d\zeta_1. \tag{51}$$

Equations (49) and (51) are solved by iterations, either analytically or numerically. In the next section the approximate analytical solution is derived. In Appendix 3 the numerical solution is described.

3.2.3 Horizontal velocity

To further simplify the problem, the IR is divided into an inner surface layer (ISL) $z_0 < z < \varepsilon l$ (where ε is a small constant), and the shear stress layer (SSL) $\varepsilon l < z < h \equiv nl$.

Inner surface layer The ISL is defined as a thin boundary layer adjacent to the surface, where the wave-induced stress is constant over height. Formally it means that the first term in the left-hand part of equation (49) is the leading one. The solution of this equation is then

$$\zeta \frac{\partial \widehat{u}_0}{\partial \zeta} = C_*, \tag{52}$$

where C_* is an unknown constant of integration proportional to the amplitude of the wave-induced shear stress inside the ISL ($\zeta < \varepsilon$). The profile of the wind velocity inside the ISL can be obtained from (52) and the lower boundary condition

$$\widehat{u}_0(\zeta_0) = \widehat{u}_s, \tag{53}$$

which results in

$$\widehat{u}_0(\zeta) - \widehat{u}_s = C_* \log(\zeta/\zeta_0). \tag{54}$$

Here $\zeta_0 = z_0/l$, and $\widehat{u}_s = \kappa c/\overline{u}_*$ is the normalized horizontal component of the orbital velocity.

Shear stress layer In the SSL all terms of equation (49) are significant. Let us rewrite equation (49) in the form

$$\frac{\partial^2}{\partial \zeta^2}(\zeta e^{-\zeta} \frac{\partial \widehat{u}_0}{\partial \zeta}) - m^2(\zeta e^{-\zeta} \frac{\partial \widehat{u}_0}{\partial \zeta}) = \Gamma_0(\zeta). \tag{55}$$

Here

$$m^2 = 2i \left(\frac{\overline{u}_* U}{\kappa |U_l|} \right) \frac{(3 - \cos^2\theta)}{(3 + \cos^2\theta)} \frac{e^{\zeta}}{\zeta},$$

and the source of vorticity $\Gamma_0(\zeta)$ is

$$\Gamma_0(\zeta) = 2 \frac{(3 - \cos^2\theta)}{(3 + \cos^2\theta)} \left(\frac{\overline{u}_* U}{\kappa |U_l|} \right) \left(\widehat{w}_1 U''_{\zeta\zeta} + i e^{-kl\zeta} U U'_{\zeta} \right). \tag{56}$$

At the upper boundary of the SSL $\zeta = n$, the solution of this equation has to patch the horizontal velocity and its vertical gradient in the OR, i.e.

$$\begin{aligned} \widehat{u}_0(n-0) &= \widehat{u}_0(n+0), \\ \left(\frac{\partial \widehat{u}_0}{\partial \zeta} \right)_{\zeta = n-0} &= \left(\frac{\partial \widehat{u}_0}{\partial \zeta} \right)_{\zeta = n+0}. \end{aligned} \tag{57}$$

At the lower boundary $\zeta = \varepsilon$ the solution of (55) has to patch the horizontal velocity in the ISL (defined by (54)) and its vertical gradient, i.e.

$$\begin{aligned} \widehat{u}_0(\varepsilon + 0) &= \widehat{u}_0(\varepsilon - 0), \\ \left(\frac{\partial \widehat{u}_0}{\partial \zeta}\right)_{\zeta=\varepsilon+0} &= \left(\frac{\partial \widehat{u}_0}{\partial \zeta}\right)_{\zeta=\varepsilon-0}. \end{aligned} \tag{58}$$

Equation (55) is an ordinary non-uniform differential equation in the variable $\zeta e^{-\zeta}\partial\widehat{u}_0/\partial\zeta$. The WKB-approximation (e.g. Nayfen, 1973) is considered as a powerful method to find the approximate solution of such a differential equation. However, direct application of this method to equation (55) is not possible, because at the critical height the function $m^2(\zeta)$ is equal to zero, which gives a singularity in the WKB solution.

To avoid the singular behaviour of the solution in the vicinity of the critical height the method by Langer (1934) (see, e.g., Nayfen, 1973) is used in the present study. The details of this method are presented in Appendix 1. According to Langer (1934) the general solution of equation (55) is

$$\zeta e^{-\zeta}\frac{\partial \widehat{u}_0}{\partial \zeta} = \frac{C}{\sqrt{\varphi'(\zeta)}} Ai(\varphi(\zeta)) + \frac{C_1}{\sqrt{\varphi'(\zeta)}} Bi(\varphi(\zeta)) + \Phi(\varphi(\zeta)). \tag{59}$$

In this equation C and C_1 are constants of integration, Ai and Bi are Airy functions (see Appendix 2), Φ is a partial solution of the non-uniform equation (55), and $\varphi(\zeta)$ is a function which obeys the equation

$$(\varphi'(\zeta))^2 = \frac{m^2}{\varphi(\zeta)}. \tag{60}$$

With the upper boundary condition (57) for $\partial\widehat{u}_0/\partial\zeta$, equation (59) can be written as

$$\zeta e^{-\zeta}\frac{\partial \widehat{u}_0}{\partial \zeta} = \frac{C}{\sqrt{\varphi'}} \frac{AiBi_n - Ai_nBi}{Bi_n} + \sqrt{\frac{\varphi'_n}{\varphi'}}(ne^{-n}G_n - \Phi_n)\frac{Bi}{Bi_n} + \Phi, \tag{61}$$

where a subscript n denotes a value at $\zeta = n$, and G_n is the vertical gradient of the horizontal velocity (defined by equation (36)) in the outer region at $\zeta = n$. The partial solution Φ is (see Appendix 1)

$$\Phi(\zeta) = -\frac{\pi}{\sqrt{\varphi'}}\left\{Ai\int_\varepsilon^\zeta (\varphi')^{-1/2} Bi\Gamma_0 d\zeta_1 - Bi\int_\varepsilon^\zeta (\varphi')^{-1/2} Ai\Gamma_0 d\zeta_1\right\}. \tag{62}$$

The function $\varphi(\zeta)$ is specified as the solution of equation (60):

$$\varphi(\zeta) = -\left[3/2\int_\zeta^\delta \sqrt{-m^2}\,d\zeta_1\right]^{2/3}, \qquad \text{if } \zeta < \delta \tag{63}$$

$$\varphi(\zeta) = \left[3/2\int_\delta^\zeta \sqrt{m^2}\,d\zeta_1\right]^{2/3}, \qquad \text{if } \zeta > \delta \tag{64}$$

with $\delta = \min(\zeta_c, n)$.

After integration of (61) with the boundary condition (57), the solution for the horizontal velocity $\widehat{u}$ is

$$\widehat{u}_0(\zeta) - \widehat{u}_{0n} = CA(\zeta) + (ne^{-n}G_n - \Phi_n)B(\zeta) - \int_\zeta^n \Phi(\zeta_1)e^{\zeta_1} d\ln\zeta_1. \tag{65}$$

In (65) the dimensionless functions $A(\zeta)$ and $B(\zeta)$ are

$$\begin{aligned} A(\zeta) &= -\int_\zeta^n \frac{AiBi_n - Ai_nBi}{Bi_n}\frac{1}{\sqrt{\varphi'}}e^{\zeta_1} d\ln\zeta_1, \\ B(\zeta) &= -\int_\zeta^n \sqrt{\frac{\varphi'_n}{\varphi'}}\frac{Bi}{Bi_n}e^{\zeta_1} d\ln\zeta_1. \end{aligned} \tag{66}$$

3.2.4 Patching the ISL and SSL solutions

To obtain the constants C and C_*, the equations for the horizontal velocity in the ISL (54) and in the SSL (65) are substituted into the lower boundary condition (58). This gives

$$C_* = \frac{(\widehat{u}_{0n} - \widehat{u}_s) + (B_\varepsilon - A_\varepsilon B'_\varepsilon/A'_\varepsilon)(ne^{-n}G_n - \Phi_n) - \int_\varepsilon^n \Phi(\zeta)e^{\zeta} d\ln\zeta}{\log(\varepsilon/\zeta_0) - A_\varepsilon/(\varepsilon A'_\varepsilon)}, \tag{67}$$

$$C = C_*/(\varepsilon A'_\varepsilon) - (ne^{-n}G_n - \Phi_n)(B'_\varepsilon/A'_\varepsilon). \tag{68}$$

Here $A_\varepsilon = A(\varepsilon)$ and $B_\varepsilon = B(\varepsilon)$, while $A'_\varepsilon = \partial A/\partial\zeta$ and $B'_\varepsilon = \partial B/\partial\zeta$ are derivatives at $\zeta = \varepsilon$. With (68) the horizontal velocity inside the SSL (65) can be written as

$$\widehat{u}(\zeta) - \widehat{u}_{0n} = C_*\frac{A(\zeta)}{\varepsilon A'_\varepsilon} + (ne^{-n}G_n - \Phi_n)\left(B(\zeta) - \frac{B'_\varepsilon}{A'_\varepsilon}A(\zeta)\right) - \int_\zeta^n \Phi(\zeta_1)e^{\zeta_1} d\ln\zeta_1. \tag{69}$$

Equations (54) and (69) define the zero-order solution of the horizontal velocity in the ISL and SSL respectively. This solution depends on the near surface friction velocity defined via the resistance law (67). The resistance law relates the surface stress (the friction velocity) to the velocity difference across the IR caused by the surface orbital velocity and wave-induced velocity in the lower part of the OR. Notice that to calculate the horizontal velocity from (69) the kl-order solution for the vertical velocity is needed.

3.2.5 Vertical velocity

The kl-order correction of the vertical velocity has a fundamental physical meaning. It gives the real part of the vertical velocity which plays a dominant role in the wave generation by the wind. Vertical motions correlated with the wave elevation produce the slope-correlated variation in the air pressure. The pressure correlated with the wave slope in turn provides the energy transfer from the air flow to the waves.

The first-order solution for the vertical velocity inside the IR follows from equation (51) with $\widehat{u}_0$ defined by (54) and (69). However, this solution does not provide the attenuation

of the vertical velocity above the IR. It is clear that such a behaviour of the vertical velocity is not physical, which is explained by the fact that the solution for $\widehat{u}_0$ used in (51) is valid for small kz only, i.e. inside the IR.

Outside the IR all wave-induced variables of the air flow decay exponentially with height. To account for this fact the exponential decay is introduced in equation (51). The equation for $\widehat{w}_1$ takes the form

$$\widehat{w}_1(\zeta) = -ikle^{-kl\zeta} \int_{\zeta_0}^{\zeta} (\widehat{u}_0 - Ue^{-kl\zeta_1}) d\zeta_1. \tag{70}$$

It is this equation which is solved by iterations together with the equation for the horizontal velocity (69).

Equation (70) is very important to understand the mechanism of wave generation. The imaginary part of the horizontal velocity, produced by the action of the shear stress inside the IR, generates the real part of the vertical velocity which is in phase with the wave elevation. This velocity penetrates into the inviscid OR and generates the slope-correlated pressure. The pressure then penetrates the thin IR and forms the energy flux from the air flow to the wave.

3.2.6 Shear stress variations

The turbulent shear stress defined by equation (45) is rewritten in the form

$$\widehat{\tau}_{13}(\zeta) = \left(\frac{3+\cos^2\theta}{3-\cos^2\theta}\right) \zeta e^{-\zeta} \frac{\partial \widehat{u}_0}{\partial \zeta}. \tag{71}$$

With (61) and (68), this equation reads

$$\widehat{\tau}_{13}(\zeta) = \left(\frac{3+\cos^2\theta}{3-\cos^2\theta}\right) \left[C_* D(\zeta) - (nG_n^i - \Phi_n) E(\zeta) + \Phi(\zeta)\right]. \tag{72}$$

The function $\Phi(\zeta)$ is defined by (62), and the functions $D(\zeta)$ and $E(\zeta)$ are

$$\begin{aligned} D(\zeta) &= \sqrt{\frac{\varphi'(\varepsilon)}{\varphi'(\zeta)}} \frac{Ai(\zeta)B_i(n) - A_i(n)B_i(\zeta)}{Ai(\varepsilon)B_i(n) - A_i(n)B_i(\varepsilon)}, \\ E(\zeta) &= \sqrt{\frac{\varphi'(n)}{\varphi'(\zeta)}} \frac{Ai(\zeta)B_i(\varepsilon) - A_i(\varepsilon)B_i(\zeta)}{Ai(\varepsilon)B_i(n) - A_i(n)B_i(\varepsilon)}. \end{aligned} \tag{73}$$

Equation (72) is valid inside the SSL ($\varepsilon < \zeta < n$). In the ISL ($\zeta_0 < \zeta < \varepsilon$) the shear stress is constant and equals

$$\widehat{\tau}_{13}(\zeta) = \left(\frac{3+\cos^2\theta}{3-\cos^2\theta}\right) C_*. \tag{74}$$

3.3 Energy transfer from wind to wave

The energy flux E_w from wind to waves is

$$\begin{aligned} \frac{\partial E_w}{\partial t} &= \langle \Upsilon_{ij} u_{si} n_j \rangle \\ &= \rho_a c \left\langle P_s \frac{\partial \eta_0}{\partial x} \right\rangle + \rho_a \langle \tau_s u_s \rangle . \end{aligned} \tag{75}$$

Here Υ_{ij} is the tensor of the total surface stress, u_{si} is a component of the surface velocity, n_j is a component of the unit vector normal to the surface, ρ_a is the air density, $P_s = P(z_0)$ is the surface pressure (including normal turbulent stresses), $\tau_s = \tau_{13}(z_0)$ is the turbulent shear stress at the surface, and brackets $\langle\rangle$ denote an average over the wave length.

The dimensionless growth rate parameter β is defined as

$$\beta = \frac{1}{E_w \omega} \frac{\partial E_w}{\partial t}, \tag{76}$$

where the gravity wave energy $E_w = 1/2 \rho_w g a^2$. In terms of normal modes this expression takes the form

$$\beta = \frac{\rho_a}{\rho_w} \frac{\overline{u}_*^2}{c^2} \left[Im(\widehat{P}_{0s}) + Re(\widehat{\tau}_s) \right], \tag{77}$$

where $\widehat{P}_{0s} = \widehat{P}_0(\zeta_0)$, and $\widehat{\tau}_s = \widehat{\tau}_{13}(\zeta_0)$. The first term in (77) describes the energy flux due to the work of pressure (and the normal Reynolds stresses) on the vertical orbital velocity; the second term represents the work of the surface tangential stress on the horizontal orbital velocity. The term $Re(\widehat{\tau}_s)$ is defined by (74) and (67). The surface pressure (and the normal stress) can be found from (11):

$$Im(\widehat{P}_{0s}) = \kappa^{-2} k \int_{z_0}^{\infty} (U \widehat{w}_{1r} - Re(\widehat{\tau}_{13}))\, dz, \tag{78}$$

where the vertical velocity is defined by (70), and the shear stress is defined by (74) and (72).

The growth rate parameter is compared with Miles (1957) theory in Section 4.3. In Miles' theory the growth rate parameter is written:

$$\beta = 2\pi \kappa^{-2} \left(-\frac{U''}{kU'} \widehat{w}^2 \right)_{z=z_c} . \tag{79}$$

With the estimate (32) of the vertical velocity at the critical height, the growth rate parameter in the inviscid shear flow is written as:

$$\beta = 2\pi \kappa^{-2} Re(\gamma)^2 k z_c \left(\int_{z_c}^{\infty} U^2 e^{-kz} dz \right)^2 . \tag{80}$$

4 Results

4.1 Wind velocity and shear stress profiles

In this section we present the comparison of the wave-induced velocity and Reynolds stress fields predicted by the simplified model with those predicted by a 2D numerical wave boundary layer model (WBL model). The latter is described in detail by Mastenbroek et al. (1996). Here we only mention that the second-order turbulence closure scheme developed by Launder et al. (1975) is used to model the turbulent stresses. Parameters of the surface wave and the air boundary layer used for the comparison are listed in Table 1. The vertical profiles of the velocity and the Reynolds stress are shown in Figures 3a-3g.

Run	U_{10}	angle	U_{10}/c	c/u_*	kz_c	kl	kz_0
1	5	0^0	0.5	60.8	1.9×10^5	0.02	5.0×10^{-6}
2	5	0^0	0.83	36.6	32.8	0.05	1.4×10^{-5}
3	5	0^0	1.66	18.3	8.5×10^{-2}	0.28	5.5×10^{-5}
4	5	0^0	5	6.1	5.7×10^{-3}	0.11	5.0×10^{-4}
5	15	0^0	0.83	28.8	2.22	0.11	1.7×10^{-5}
6	15	0^0	1.66	14.4	2.5×10^{-2}	0.17	6.8×10^{-5}
7	15	180^0	1.5	15.9	–	0.03	5.6×10^{-5}

Table 1: Parameters for different test runs

In the OR ($kz > kl$) the structure of the velocity field reflects the properties of the inviscid shear flow above a wavy surface. Here the wave-induced motion is defined mainly by the elevation-correlated (real part) component of the horizontal velocity and the slope-correlated (imaginary part) component of the vertical velocity. Their quadrature components ($Im(\hat{u})$ and $Re(\hat{w})$ respectively) are negligible in the OR. A good agreement of the approximate solution based on equations (34) and (36) with the numerical solution based on 2D WBL model is found for all 7 cases.

In run 1 (Figure 3a) the surface wave runs faster than the wind. At sea this case corresponds to swell. The critical height is located outside the wave boundary layer. The structure of the IR is determined by turbulent stresses. The main role of turbulent viscosity in the IR is that it provides the patching of the air flow fluctuations to the orbital velocities of the surface wave. This results in the generation inside the IR of the slope-correlated horizontal velocity, and hence (through the continuity equation) the elevation-correlated component of the vertical velocity. The latter is small (kl-order) but plays a crucial role in the energy and momentum exchange between wind and waves. The vertical profiles of turbulent shear stress obtained by the simplified and the numerical model are in qualitative and quantitative agreement. Both models predict a strong enhancement of surface stresses in the region of the wave trough.

The wave in run 2 (Figure 3b) corresponds to the peak of the wind wave spectrum of a fully developed sea characterised by inverse wave age $U_{10}/c = 0.83$. The features of the air

flow are qualitatively the same as for case 1. Again the comparison between the simplified and the numerical model is reasonable both in the outer and in the inner region.

Case 3 (Figure 3c) corresponds to a surface wave of which the frequency is twice that of the peak of a fully developed sea spectrum. The height of the IR $kl = 0.27$ is close to its maximal value (see Figure 1). In this case it could be expected that the solution of the simplified model deviates from the numerical solution as the accuracy of our approximation is of kl-order. An additional complication could arise from the fact that the critical height $kz_c = 0.084$ is comparable to the height of the IR. However, the comparison is encouraging. The simplified model reproduces well the local maximum in $Re(\widehat{u})$ and the local minimum in stresses in the vicinity of the IR height $kz = 0.3$. These extremes are generated by the vertical advection of vorticity.

Run 4 (Figure 3d) corresponds to a slow wave. Again a good comparison in velocity distributions is found. The structure of the IR is characterized by a speed-up of the horizontal velocity over the crest. The horizontal acceleration of the air flow occurs in the vicinity of the IR height and is caused by the source of vorticity: just on this level the real part of the vertical velocity has its maximum. The numerical model gives a somewhat stronger acceleration of the flow than the simplified model. This is explained by the fact that the turbulent mixing in the numerical model at the upper boundary of the IR is more suppressed than in the simplified model. The vertical profiles of the turbulent shear stress are in qualitative agreement, though the local extreme of $Re(\widehat{\tau})$ is underestimated by the simplified model. Furthermore, the simplified model cannot reproduce the existence of slope-correlated stress in the OR.

While runs 1 to 4 had low wind speeds, runs 5 and 6 (Figure 3e and 3f) illustrate the case of strong wind. Here, the inverse wave age is the same as in runs 2 and 3 respectively. The model calculations give similar results as were obtained for low wind (compare Figures 3b and 3e, and Figures 3c and 3f). This shows that the structure of the wave-induced fields is defined mainly by the wave age of a wave component, rather than by the wind speed itself. A reasonable agreement between the solution of the simplified and the numerical models can be noticed.

Finally, case 7 (Figure 3g) is related to swell which propagates against the wind. In this case the horizontal velocity speed-up occurs over the crest of the wave. Inside the IR the action of turbulent stresses shifts the region of the accelerated air flow to the downwind slope. The maximum of surface stresses is in the vicinity of the wave crest, but is shifted to the downwind slope. Remarkabley, the simplified description of the turbulent wave boundary layer is well consistent with the complicated 2D WBL model.

The main conclusion can be drawn from a comparison between the models. The general peculiarities of the air flow dynamics over surface waves for a wide range of phase velocities (from waves running faster than the wind to waves running much more slowly than the wind) can be reproduced both qualitatively and quantitatively with the use of a simplified description which is conceptually based on the division of the turbulent wave boundary layer into two parts: the outer region and the inner region. The description of the air flow in the OR is based on the solution of the Rayleigh and the vorticity equation for inviscid shear flow. In the IR the wave-induced motions are found through solution of the vorticity

equation in which the turbulent diffusion of vorticity is taken into account.

For a correct parameterisation of turbulence in the OR it is only important that variations in turbulent stresses are suppressed. Which turbulence closure is chosen to provide this suppression is not important: whether it is a complicated second-order closure scheme or a primitive vertical damping of turbulent stresses, as is used in the simplified model.

4.2 Comparison with measurements

In this section results of the simplified model are compared with the laboratory measurements of velocity and stress fields by Hsu and Hsu (1983). They used a mechanically generated wave with phase velocity 1.6 m/s. Other parameters of three runs of this experiment are shown in Table 2. In this table U_∞ is the wind speed in the middle of the tank.

Run	U_∞ (m/s)	$u_{*\mathrm{exp}}$ (m/s)	$U(k^{-1})$ (m/s)	u_* (m/s)	$U(k^{-1})/c$
1	1.37	0.043	1.4	0.06	0.87
2	2.12	0.073	2.0	0.08	1.28
3	2.92	0.110	2.9	0.13	1.84

Table 2: Parameters of the experiment of Hsu and Hsu (1983)

The wind velocity at $z = k^{-1}$, denoted by $U(k^{-1})$, and the friction velocity u_* presented in Table 2 are determined by fitting a logarithmic profile to the observed mean wind speed.

The wave-induced horizontal velocity and shear stresses measured in a wave following coordinate system are shown in Figures 4a-4c. The vertical velocity is not shown in the figures as there is an apparent bias in these data of which the cause is unknown (Mastenbroek, 1996).

Runs 1 and 2 relate to cases where the wave moves somewhat more slowly and faster than the wind respectively; run 3 represents a slowly propagating wave. In cases 1 and 3 the measurements were done in both outer and inner regions, while in case 2 the IR depth is large, and all measurements are confined to the inner region.

The data confirm the existence of the outer and inner regions. Neither case 1 nor case 2 exhibits any significant variations in the turbulent shear stress inside the OR, while inside the IR a systematical trend in the shear stresses is clearly seen. In run 2 all measurements are done inside the IR, and the stress varies throughout the whole domain.

Peculiarities of the wave-induced horizontal velocity are determined by the phase speed of the wave (or more correctly: by the wave age parameter). If the wave runs faster than the wind, then the air flow accelerates above the trough (run 1). Otherwise, the air flow accelerates over the crest (runs 2 and 3): the larger the speed difference between wind and wave, the stronger the acceleration.

The simplified model reproduces well the behaviour of the wave-induced disturbances of the velocity and stress fields above the wave. The only significant deviation of model

predictions from laboratory data can be observed in the lower part of the vertical profile of $Re(\hat{\tau})$.

4.3 Comparison of predicted growth rate with WBL-model and Miles' theory

In Figure 5 a comparison of the growth rate parameter resulting from the simplified model, the WBL model and the theory of Miles (1957) (see Section 3.3) is shown. In the IR the air flow dynamics is governed mainly by the shear stresses. They generate the real part of the vertical velocity (in kl-order, see equation (70)), which in turn generates the slope correlated surface pressure (78) in the OR. This pressure penetrates the thin IR and forms the energy flux to waves (sheltering mechanism of wave generation). The magnitude of $Re(\hat{w}_1)$ and hence $Im(\hat{P}_{0s})$ is less than that predicted by Miles theory, which results in smaller values of β. In the range $15 < c/u_* < 22$ the growth rate has a peak. Its origin can be explained by the fact that in this range of c/u_* the critical height approaches the upper boundary of the IR, and peculiarities of the critical layer dynamics (though they are still suppressed by the weakened turbulence) become important. In the range of fast waves the growth rate parameter is negative; it means that waves return their momentum to the air flow.

Qualitatively, the simplified model reproduces well the growth rate dependence on c/u_* resulting from the numerical WBL-model. There is only a small underestimation of β.

It is rather surprising that Miles' theory predicts the largest values of β for slowly moving waves ($c/u_* < 15$), and is in better agreement with empirical values of the growth rate parameter (Plant, 1982). It was shown in Section 2.2.1 that the applicability of the quasi-linear theory is restricted to a very narrow range of the inverse wave age around $U_{10}/c \simeq 1.2$. Outside this range the critical height is inside the IR and its singular behaviour must be significantly suppressed by the action of turbulent stresses. Comparison of the wave-induced velocity resulting from Miles' theory with the measurements of Hsu and Hsu (1983), clearly shows that this theory does not hold.

A comparison of the angular distribution of the growth rate $\beta(\theta)$ predicted by the simplified and the WBL model for inverse wave ages $U_{10}/c = 1.5$ and 5 is presented in Figure 6. Both models predict a widening of the angular dependence of β with an increase in the wind speed. For the fast wave the simplified model is well consistent with the numerical model. For the slow wave the simplified model gives a more rapid drop of β with increasing angle than the numerical model.

5 Discussion and conclusions

A simplified model of the wave boundary layer over a surface wave propagating at an arbitrary phase velocity (as compared to the wind speed) and direction (relative to the wind direction) has been presented. The main simplification of the problem is achieved by the division of the wave boundary layer into an outer (OR) and an inner (IR) region. In the OR the wave-induced motions experience inviscid undulation, while in the IR they are strongly affected by the turbulent shear stresses.

The IR depth is relatively small ($kl \sim 0.1$) for all waves, except for those running with a phase speed close to the wind velocity (wave age is $1 < U_{10}/c < 1.2$). In this narrow range the height of the IR is $kl \sim 1$. An important conclusion resulting from the analysis of the IR depth is that the critical height (the height where the wind speed equals the phase velocity of the wave) is almost always located inside the IR. This means that the singular behaviour of the critical layer dynamics is strongly suppressed by the turbulent stresses for all waves, with exception of those with a wave age close to $U_{10}/c \approx 1.2$.

The fact that the singular behaviour of the critical layer dynamics does not influence the inviscid outer region, allows a simple description of the wind velocity in the OR. This description is based on the approximate solution of the Rayleigh equation suggested by Miles (1957). The solution for the vertical velocity is proportional to the mean wind velocity and an exponential decay function. The approximate solution for the horizontal velocity results from the integration of the inviscid vorticity equation with known vertical velocity. The description of the OR in the simplified model is presented by explicit formulas, and is compared with the results of the numerical solution of the Rayleigh equation. A good comparison is found.

The description of the IR is based on the solution of the vorticity conservation equation which accounts for the turbulent diffusion of vorticity. The turbulent shear stresses are parameterised using the mixing length closure theory. Introduction of exponential vertical damping of the wave-induced shear stress leads to further simplification of the problem. The damping of the shear stress describes phenomenologically the basic feature of the wave boundary layer: the rapid distortion of turbulence in the OR. The zero-order solution (in terms of a kl-power expansion) of the vorticity equation is found. Explicit relations for the wind velocity and the shear stress inside the IR are found and patched with the OR solution.

Correction of the IR solution in kl-order only has a physical significance for the real part of the vertical velocity. This component of the vertical motion, being generated inside the IR due to the action of the shear stress, penetrates into the OR, and generates the slope correlated component of the air pressure there. This pressure penetrates the thin IR and forms the energy and momentum flux from wind to waves (the so-called sheltering mechanism of wave generation).

The comparison of results obtained by the simplified and the numerical 2D WBL model is encouraging. Reasonable agreement is found between the wave-induced velocity, the shear stress and the growth rate parameter. This result has a very important consequence: the description of the air flow dynamics over waves appears not to be sensitive to the details

of the turbulence closure scheme. For a correct description of the air flow a scheme only has to provide the vertical damping of the wave-induced stresses at a scale comparable with the IR height. The phenomenological approach used in this paper is based on a direct suppression of the turbulent stresses with height. This gives results which are close to those found by using the complicated second-order Reynolds stress closure scheme developed by Launder et al. (1975).

The results of the simplified model are consistent with data of Hsu and Hsu (1983) obtained in a laboratory experiment. The experimental data confirm the existence of the outer (and the inner) region above waves.

Acknowledgements

For V.K. and V.M. this research was supported by the Office of Naval Research (ONR Grant Number N00014-98-1-0437 and N00014-98-1-0653; PR number 98PR04572-00 and 98PR05889-00), by the EU Environment Programme (Contract ENV4-CT97-0460, ASPEN) and by INTAS-International Association (Reference number INTAS-CNES 97-0222), whom they gratefully acknowledge. J-F.M. was supported by the Netherlands Organization for Scientific Research (NWO). V.K. would like to thank the staff of the Applications and Models Division and the Oceanographic Division for their hospitality during his visits to KNMI as a guest researcher. It is also a pleasure to acknowledge Dr. Gerbrand Komen for numerous helpful discussions, and for providing us with the code for the numerical solution of the Rayleigh equation.

A Appendices

A.1 Langer's method

We search for the approximate solution of equation (55), which we write as:

$$\frac{\partial^2 \tau}{\partial \zeta^2} - m^2(\zeta)\tau = f(\zeta), \tag{81}$$

with $\tau = \zeta e^{-\zeta}\partial \widehat{u}_0/\partial\zeta$ and $f = \Gamma_0$. We use an approach developed by Langer (1934), which allows to avoid the singular behaviour of the solution in the point ζ_c, where $m^2(\zeta_c) = 0$ (the so-called turning point). Following Langer's method, we introduce new independent variables:

$$\eta = \varphi(\zeta) \text{ and } v = \psi(\zeta)\tau(\zeta). \tag{82}$$

Then equation (81) takes the form:

$$\frac{\partial^2 v}{\partial \eta^2} + (\varphi')^{-2}(\varphi'' - 2\varphi'\psi'/\psi)\frac{\partial v}{\partial \eta} + (\varphi')^{-2}\left(-m^2 - \psi(\psi'/\psi^2)'\right)v = f\psi(\varphi')^{-2} \tag{83}$$

The functions $\varphi(\zeta)$ and $\psi(\zeta)$ are chosen so that

$$\begin{aligned} \psi &= \sqrt{\varphi'}, \\ \frac{m^2}{(\varphi')^2} &= \varphi. \end{aligned} \tag{84}$$

Then equation (83) becomes

$$\frac{\partial^2 v}{\partial \eta^2} - \eta v = f(\varphi')^{-3/2}. \tag{85}$$

In this equation the term δv is omitted, where $\delta = -3/4(\varphi'')^2(\varphi')^{-4} + 1/2\varphi'''(\varphi')^3$. It is assumed that the omitted term is significantly less than ηv.

The general solution of equation (85) is

$$v = C_1 Ai(\eta) + C_2 Bi(\eta) + \Psi(\eta), \tag{86}$$

where Ai and Bi are Airy functions (see Appendix 2), and Ψ is a partial solution of the non-uniform equation (85). The partial solution can be obtained through the Green function G:

$$\Psi(\eta) = \int_0^\infty G(x,\eta) f(x)(\varphi'(x))^{-3/2} dx.$$

The Green function for equation (85) is

$$G(x,\eta) = \pi\left[Ai(x)Bi(\eta) - Ai(\eta)Bi(x)\right] H(\eta - x), \tag{87}$$

where $H(\eta - x)$ is the Heavyside function, defined as $H = 0$, if $\eta - x < 0$ and $H = 1$, if $\eta - x > 0$.

A.2 Airy functions

The Airy functions Ai and Bi are independent solutions of the following differential equation (Abramowitz and Stegun, 1964)

$$\frac{\partial^2 v}{\partial z^2} - zv = 0.$$

Their integral presentation is:

$$\begin{aligned}(3a)^{-1/3}\pi Ai\left[\pm(3a)^{-1/3}z\right] &= \int_0^\infty \cos(at^3 \pm zt)dt \\ (3a)^{-1/3}\pi Ai\left[\pm(3a)^{-1/3}z\right] &= \int_0^\infty \left[\exp(-at^3 \pm zt) + \cos(at^3 \pm zt)dt\right] dt.\end{aligned}$$

In the present study the Airy functions are used to find the approximate solution inside the IR. In this region the variable z is limited by the condition $|z| < 2$. For convenience of calculation the Airy functions in this range of z can be presented in ascending series:

$$\begin{aligned}Ai(z) &= c_1 f(z) - c_2 g(z), \\ Bi(z) &= \sqrt{3}(c_1 f(z) + c_2 g(z)).\end{aligned}$$

Here $c_1 = 0.35502$ and $c_2 = 0.25882$ are constants, and the functions f and g are defined as:

$$\begin{aligned}f(z) &= \sum_0^N 3^k (\frac{1}{3})_k \frac{z^{3k}}{(3k)!}, \\ g(z) &= \sum_0^N 3^k (\frac{2}{3})_k \frac{z^{3k+1}}{(3k+1)!},\end{aligned}$$

where $(\alpha+1/3)_0 = 1$ and $3^k(\alpha+1/3)_k = (3\alpha+1)(3\alpha+4)\cdots(3\alpha+3k-2)$, for $k = 1, 2, 3, \ldots$ (with $\alpha = 0$ and $\alpha = 1/3$ in the f and g series respectively).

A.3 Numerical solution

Equation (56) gives a second-order ordinary differential equation in the variable $\zeta e^{-\zeta}\partial\hat{u}_0/\partial\zeta$. Instead of an approximation with Airy-functions, it can also be solved by a numerical method. In this case it is more convenient to remove the inner surface layer, so that the equation is solved from $\zeta = \zeta_0$ to $\zeta = n$. Then two boundary conditions are needed. At $\zeta = n$, the solution has to patch the OR-solution (Eq. (58)). However, at $\zeta = \zeta_0$ no direct boundary condition is available. Therefore the following procedure is applied:

1. A first guess for $\partial\hat{u}_0/\partial\zeta$ at $\zeta = \zeta_0$ is taken.

2. Eq. (56) is solved numerically.

3. The profile of the horizontal velocity gradient found in this way is integrated from the surface to the top of the SSL, starting with the lower boundary condition $\hat{u}_0(\zeta_0) = \hat{u}_s$. This results in a value of $\hat{u}_0(n-0)$.

4. Dependent on the difference $\hat{u}_0(n+0) - \hat{u}_0(n-0)$, the lower boundary condition for $\partial\hat{u}_0/\partial\zeta$ is changed and the iteration is repeated from step 2.

The iteration is continued until $\hat{u}_0(n+0) - \hat{u}_0(n-0)$ is small enough.

References

[1] Belcher, S.E., and J.C.R. Hunt, 1993, Turbulent shear flow over slowly moving waves, *J. Fluid Mech.*, 251, 109-148.

[2] Belcher, S.E., and J.C.R. Hunt, 1998, Turbulent flow over hills and waves, *Annu. Rev. Fluid Mech.*, 30, 507-538.

[3] Hsu, C.T., and Y. Hsu, 1983, On the structure of turbulent flow over a progressive water wave: theory and experiment in a transformed, wave-following coordinate aystem. Part 2, *J. Fluid Mech.*, 131, 123-153.

[4] Hunt, J.C.R., S. Leibovich, and K.J. Richards, 1988, Turbulent shear flow over low hills, *Q.J.R. Met. Soc.*, 114, 1435-1471.

[5] Harris, J.A., S.E. Belcher, and R.L. Street, 1996, Linear dynamics of wind waves in coupled turbulent air-water flow: Part 2, *J. Fluid Mech.*, 308, 219-254.

[6] Komen, G.J., L. Cavaleri, M. Donelan, K. Hasselmann, S.Hasselmann and P.A.E.M. Janssen, 1994, *Dynamics and modelling of ocean waves*, Cambridge Univ. Press, 540p.

[7] Kudryavtsev, V.N., C. Mastenbroek, and V.K. Makin, 1997. Modulation of wind ripples by long surface waves via the air flow: A feedback mechanism, *Boundary-Layer Meteor.*, 83, 99-116.

[8] Launder, B.E., G.J. Reece, and W. Rodi, 1975, Progress in the development of a Reynolds-stress turbulence closure, *J. Fluid Mech.*, 16, 138-159.

[9] Lighthill, M.J., 1957, The fundamental solution for small steady three-dimensional disturbances to a two-dimensional parallel shear flow, *J. Fluid Mech.*, 3, 1-13.

[10] Mastenbroek, C., V.K. Makin, M.H. Garat, and J.P. Giovanangeli, 1996, Experimental evidence of the rapid distortion of turbulence in the air flow over water waves, *J. Fluid Mech.*, 318, 273-302.

[11] Miles, J.W., 1957, On the generation of surface waves by shear flow, *J. Fluid Mech.*, 3, 185-204.

[12] Miles, J.W., 1959, On the generation of surface waves by shear flows. Part 2, *J. Fluid Mech.*, 6, 568-582.

[13] Miles, J.W., 1962, On the generation of surface waves by shear flows. Part 4, *J. Fluid Mech.*, 13, 433-448.

[14] Phillips, O.M., 1966, *The dynamics of the upper ocean*, Cambridge Univ. Press, 261p.

Figures

Figure 1. Vertical structure of the turbulent boundary layer over a wave as a function of U_k/c for wind speed $U_{10} = 5$ m/s (frame a) and $U_{10} = 15$ m/s (frame b). The solid line is the IR scale kl (equation (21)); the dashed line is the critical height kz_c (equation (14)); the dotted line is the roughness scale kz_0 (equation (15)).

Figure 2. Inviscid shear flow: profiles of real and imaginary parts of vertical ($\widehat{w}(x_3)$) and horizontal ($\widehat{u}(x_3)$) velocities. The wind speed $U_{10} = 15$ m/s. The inverse wave age parameter is $U_{10}/c = 2$ (left column), and $U_{10}/c = 5$ (right column). The approximate solution (equations (34) and (36)) is shown by dashed lines. The solid lines show the numerical solution of the Rayleigh equation (29) with the horizontal velocity defined through the continuity equation (5). Wind velocities are normalized on $ak\overline{u}_*/\kappa$. The critical height is kz_c=0.018 for $U_{10}/c = 2$, and $kz_c = 0.004$ for $U_{10}/c = 5$.

Figure 3a. Profiles of real and imaginary parts of the horizontal velocity (left column), the vertical velocity (middle column), and the shear stress (right column). The solid lines show the solutions of the simplified model for $\widehat{u}(z)$, $\widehat{w}(z)$, and $\widehat{\tau}(z)$ (equations (65), (70), and (72) respectively); the dashed lines show the results of numerical calculations based on the 2D wave boundary layer model with the second-order closure scheme (Mastenbroek et al., 1996); the dotted lines represent the simplified model solution obtained with the numerical method (see Appendix 3). Wind speed is $U_{10} = 5$ m/s; inverse wave age is $U_{10}/c = 0.5$. Wind velocities are normalized on $ak\overline{u}_*/\kappa$, and the shear stress is normalized on $ak\overline{u}_*^2$.

Figure 3b. The same as in Figure 3a, but $U_{10} = 5$ m/s and $U_{10}/c = 0.83$.

Figure 3c. The same as in Figure 3a, but $U_{10} = 5$ m/s and $U_{10}/c = 1.66$.

Figure 3d. The same as in Figure 3a, but $U_{10} = 5$ m/s and $U_{10}/c = 5.0$.

Figure 3e. The same as in Figure 3a, but $U_{10} = 15$ m/s and $U_{10}/c = 0.83$.

Figure 3f. The same as in Figure 3a, but $U_{10} = 15$ m/s and $U_{10}/c = 1.66$.

Figure 3g. The same as in Figure 3a, but for a wave moving opposite to the wind. Wind speed is $U_{10} = 15$ m/s and inverse wave age is $U_{10}/c = 1.5$.

Figure 4a. Comparison of the simplified model results (solid lines) with laboratory measurements of Hsu and Hsu (1983), shown by open squares. Run 1: $U_k = 1.4$ m/s; $U_k/c = 0.87$ (see Table 2 for details). The horizontal velocity is normalized on $ak\overline{u}_*/\kappa$, and the shear stress is normalized on $ak\overline{u}_*^2$.

Figure 4b. The same as in figure 4a. Run 2: $U_k = 2.0$ m/s and $U_k/c = 1.28$.

Figure 4c. The same as in figure 4a. Run 3: $U_k = 2.9$ m/s and $U_k/c = 1.84$.

Figure 5. Growth rate parameter as a function of $\overline{u}_*/c$ for different models. The solid line denotes the solution of the simplified model for $U_{10} = 5$ m/s (squares), and $U_{10} = 15$ m/s (triangles); the dashed line relates to the solution of the 2D numerical model (Mastenbroek et al., 1996); the dash-dotted line represents the solution of the quasi-laminar model of Miles (1957).

Figure 6. Angular dependence of the growth rate parameter at $U_{10} = 15$ m/s. Inverse wave age $U_{10}/c = 5$ (upper frame) and $U_{10}/c = 1.5$ (lower frame). Solid lines correspond to the simplified model, dashed lines to the 2D numerical model.

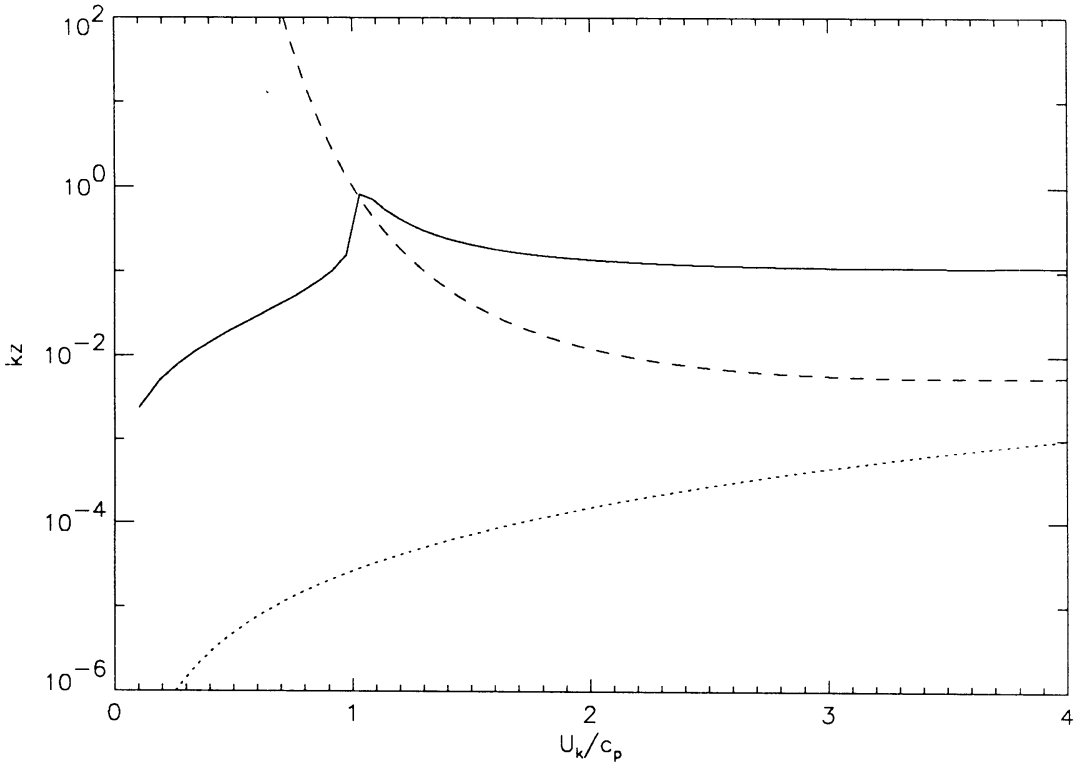

Figure 1a

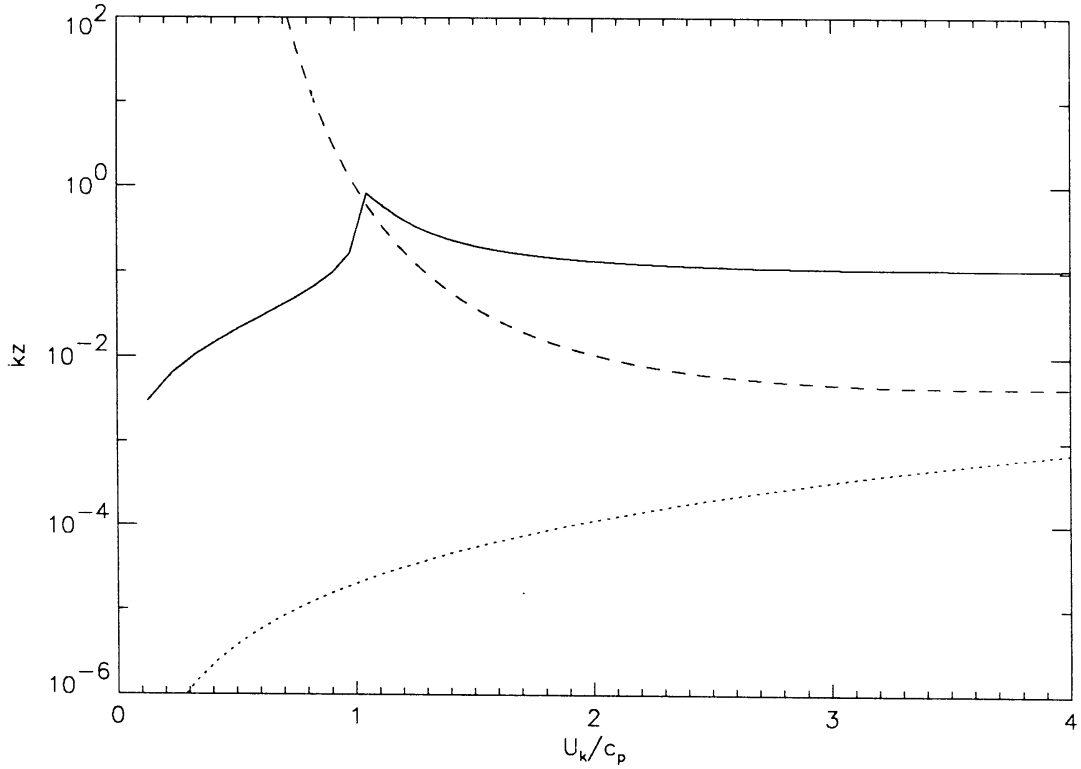

Figure 1b

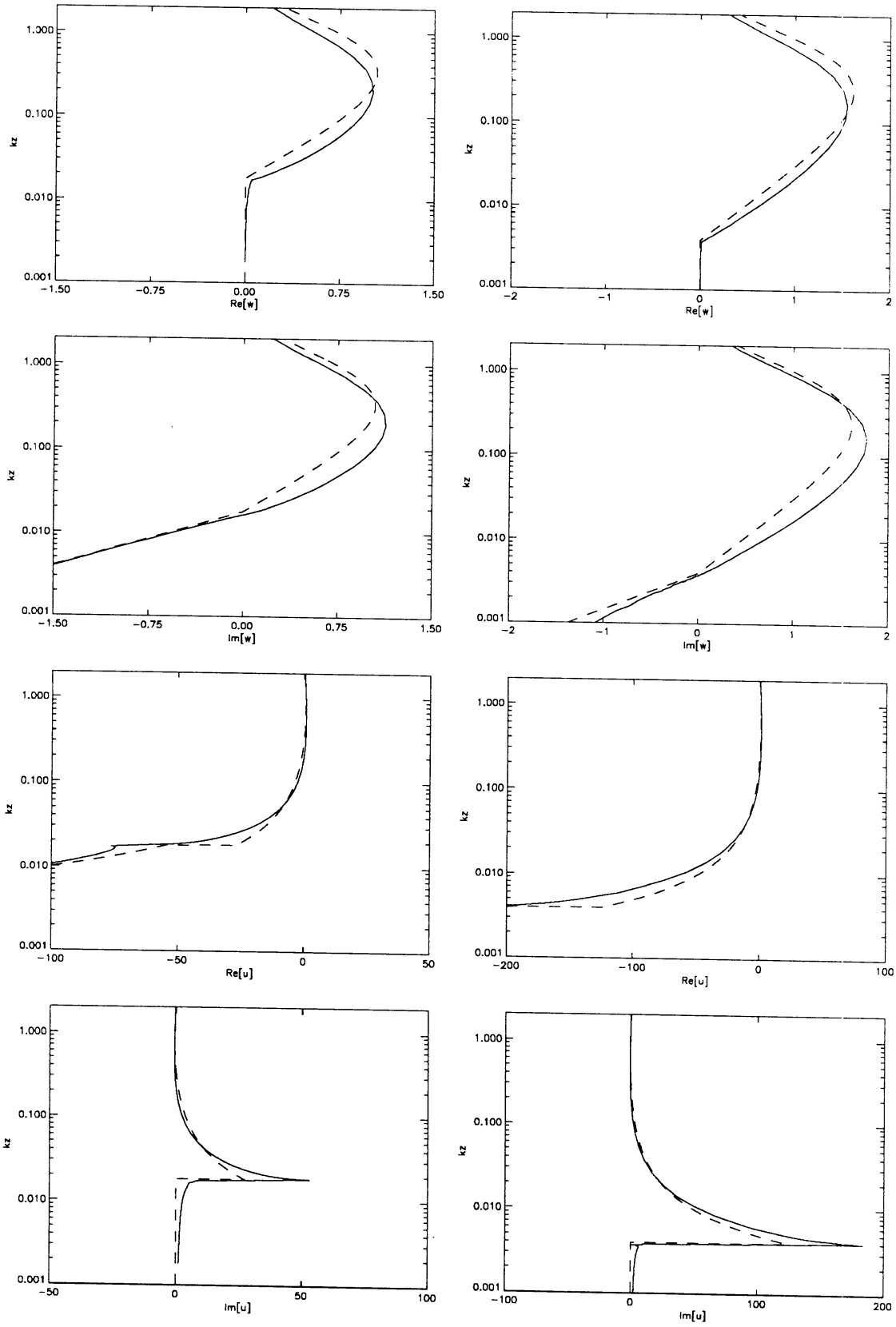
kz
1.000
0.100
0.010
0.001
−1.50
−0.75
0.00
0.75
1.50
Re[w]
−2
−1
0
1
2
Re[w]
Im[w]
Im[w]
−100
−50
0
50
Re[u]
−200
−100
0
100
Re[u]
−50
0
50
100
Im[u]
−100
0
100
200
Im[u]

Figure 2

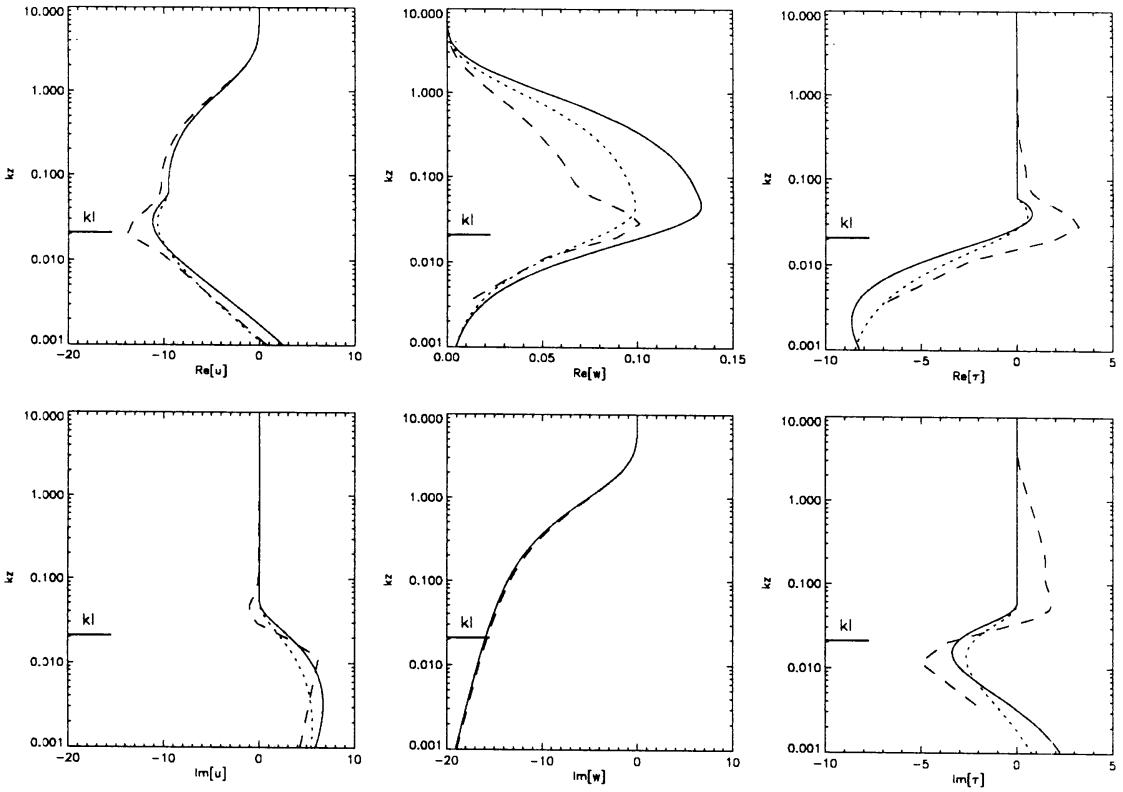

Figure 3a

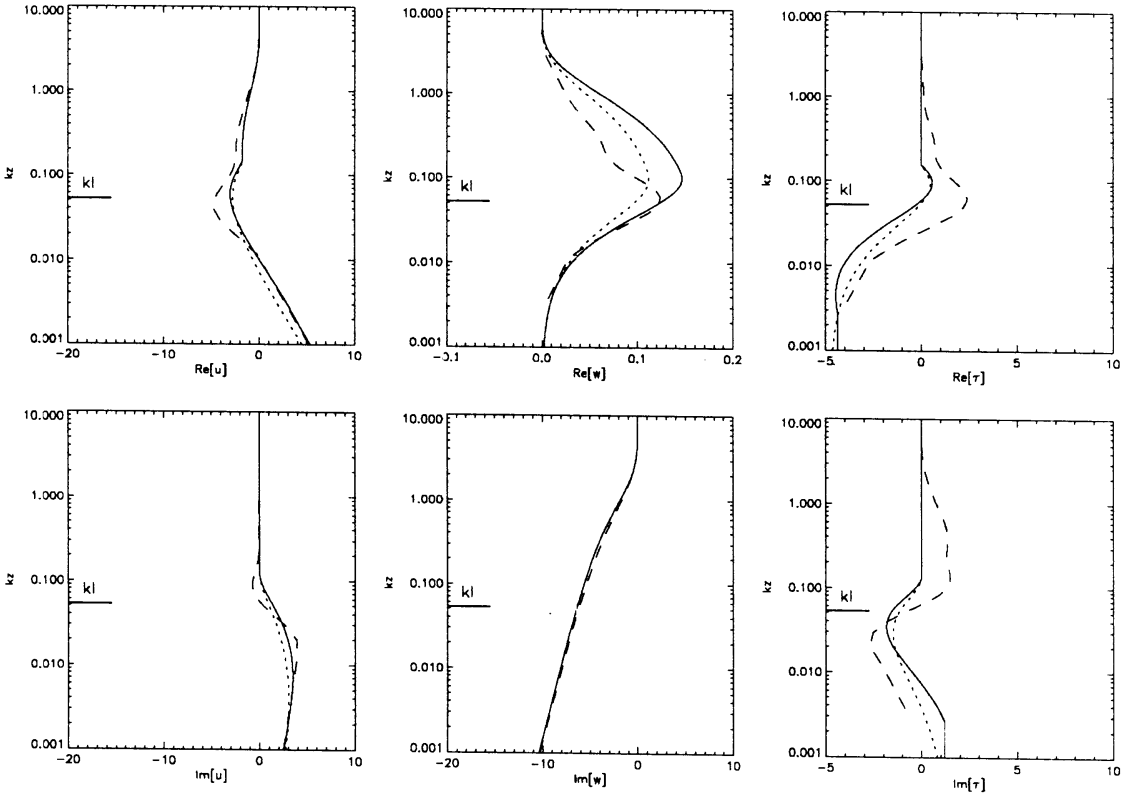

Figure 3b

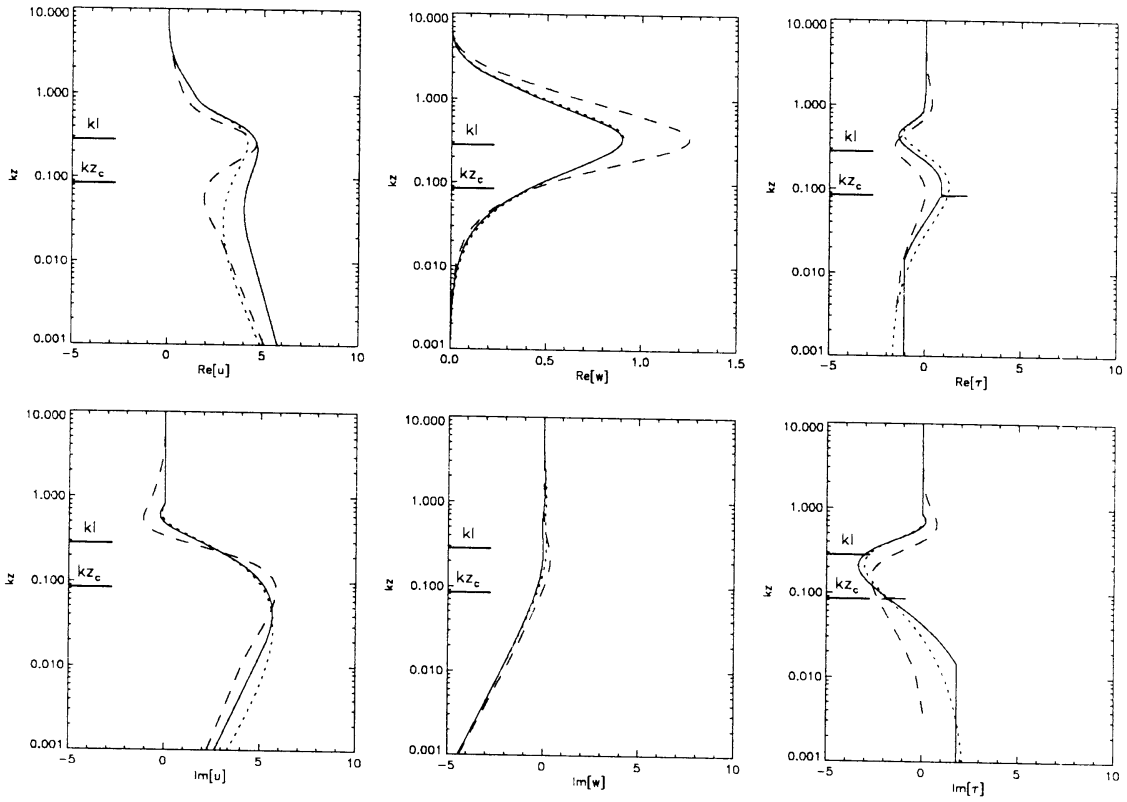

Figure 3c

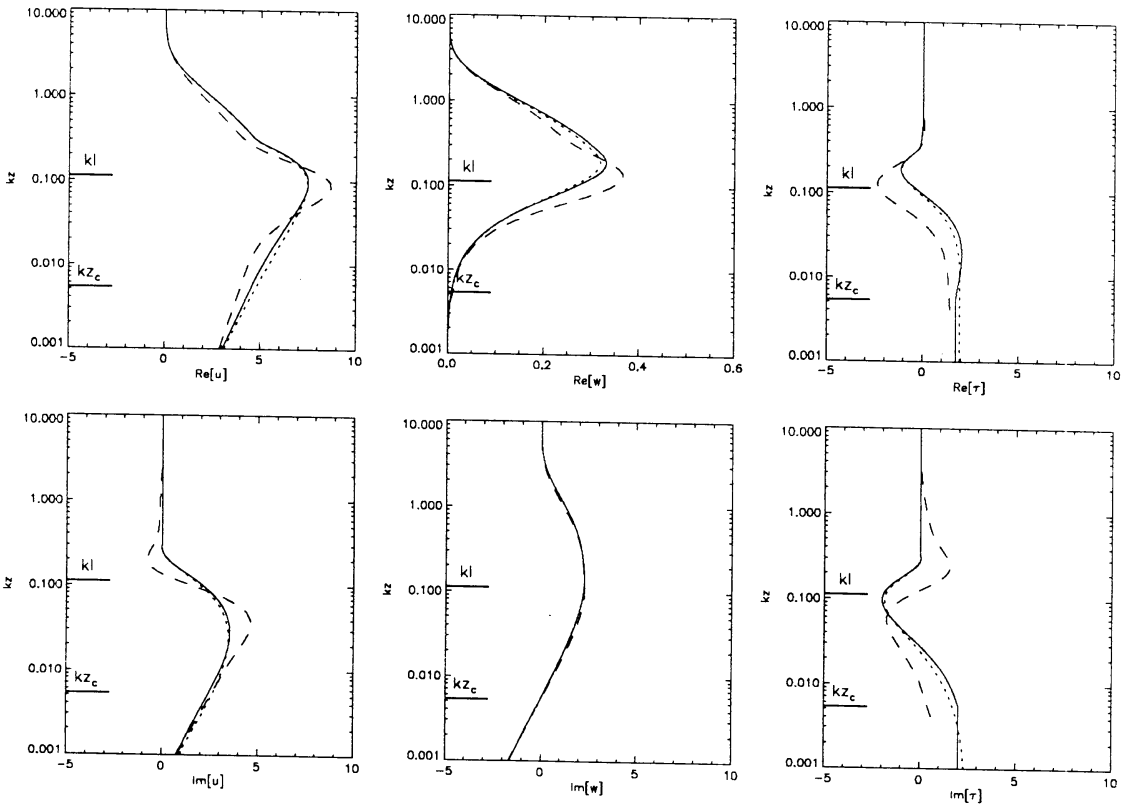

Figure 3d

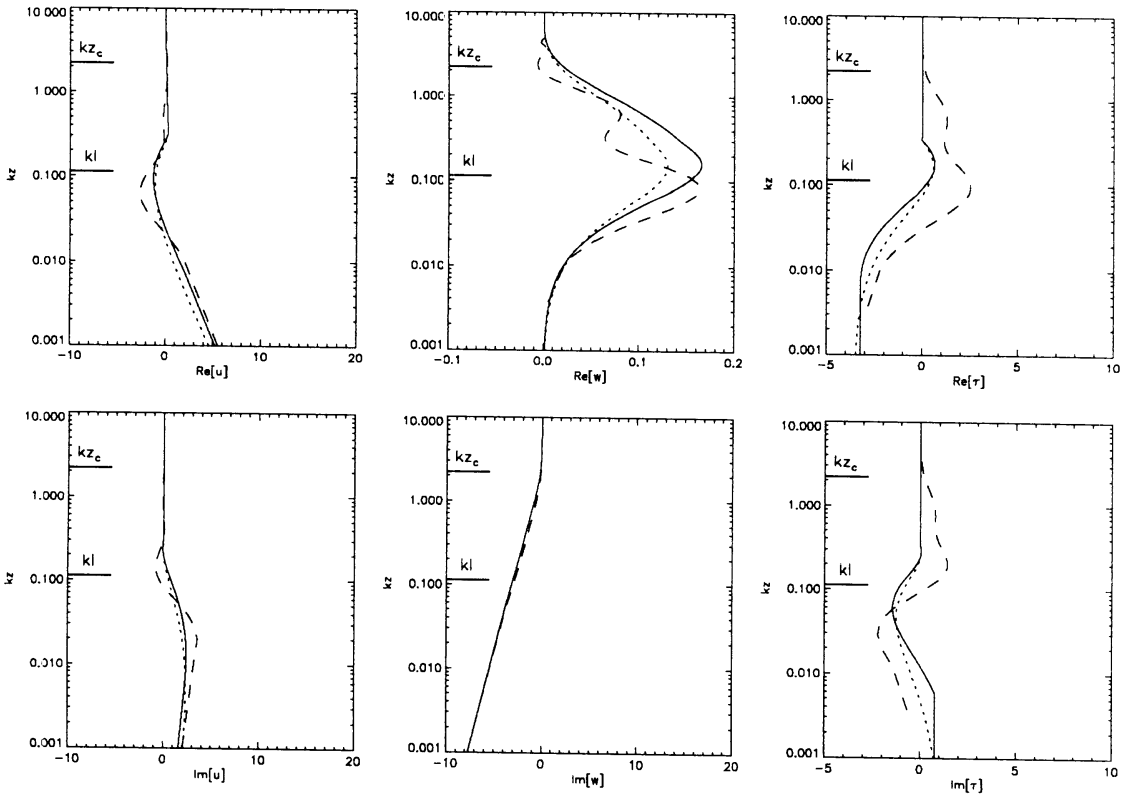

Figure 3e

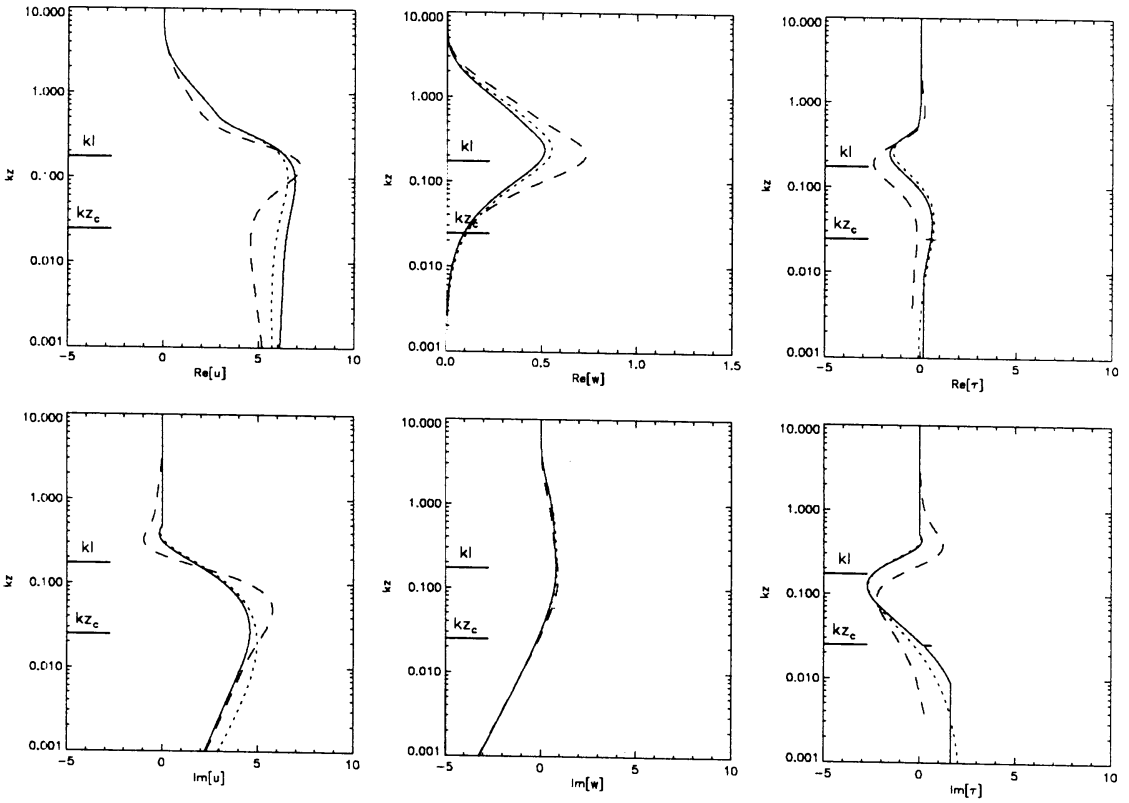

Figure 3f

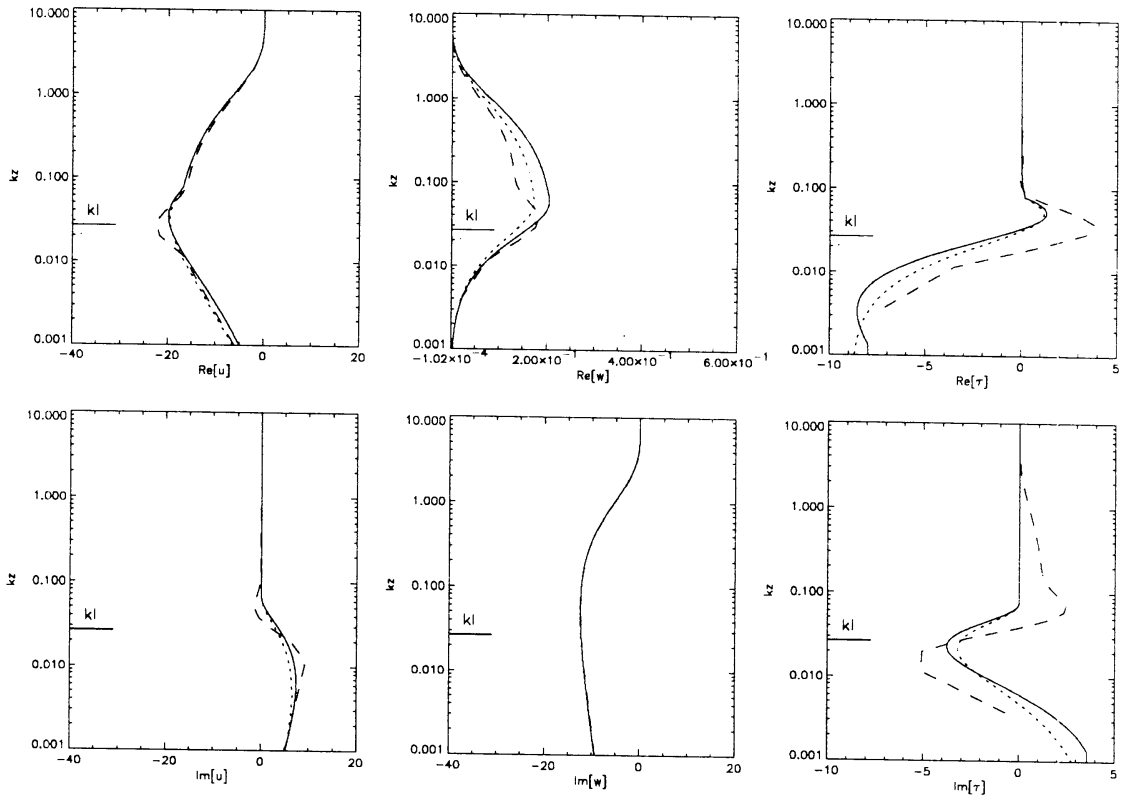
10.000
1.000
0.100
0.010
0.001
kz
kl
−40
−20
0
20
Re[u]
−1.02×10⁻⁴
2.00×10⁻¹
4.00×10⁻¹
6.00×10⁻¹
Re[w]
−10
−5
0
5
Re[τ]
Im[u]
Im[w]
Im[τ]

Figure 3g

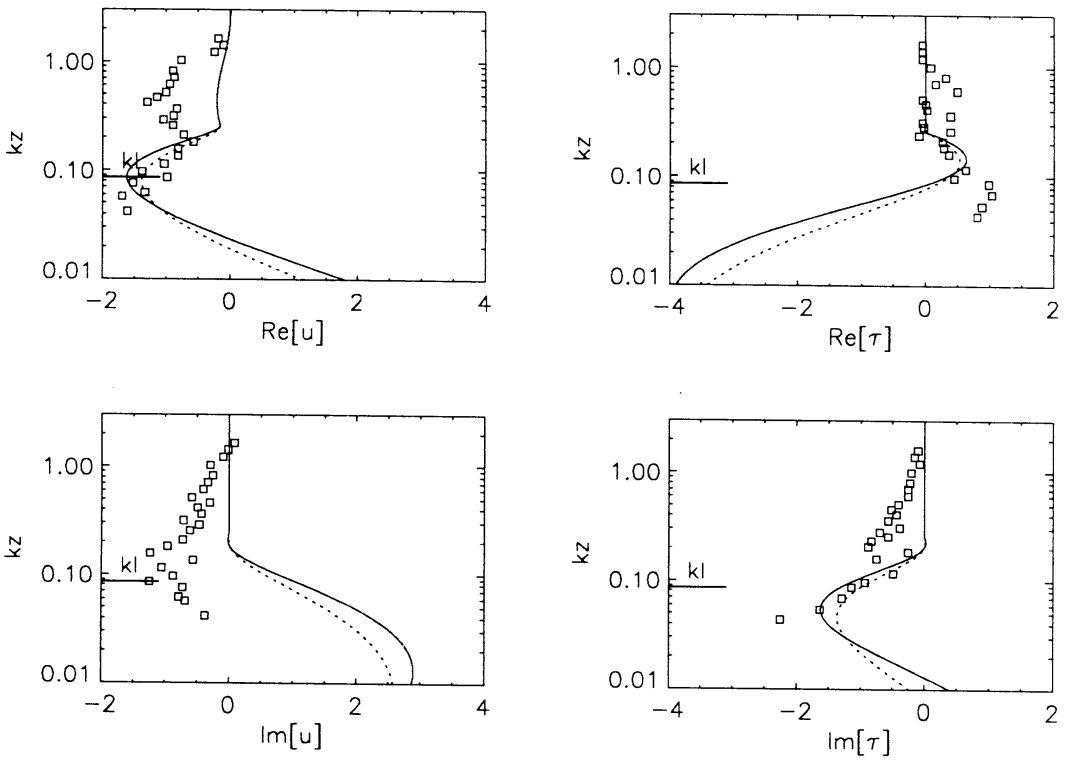

Figure 4a

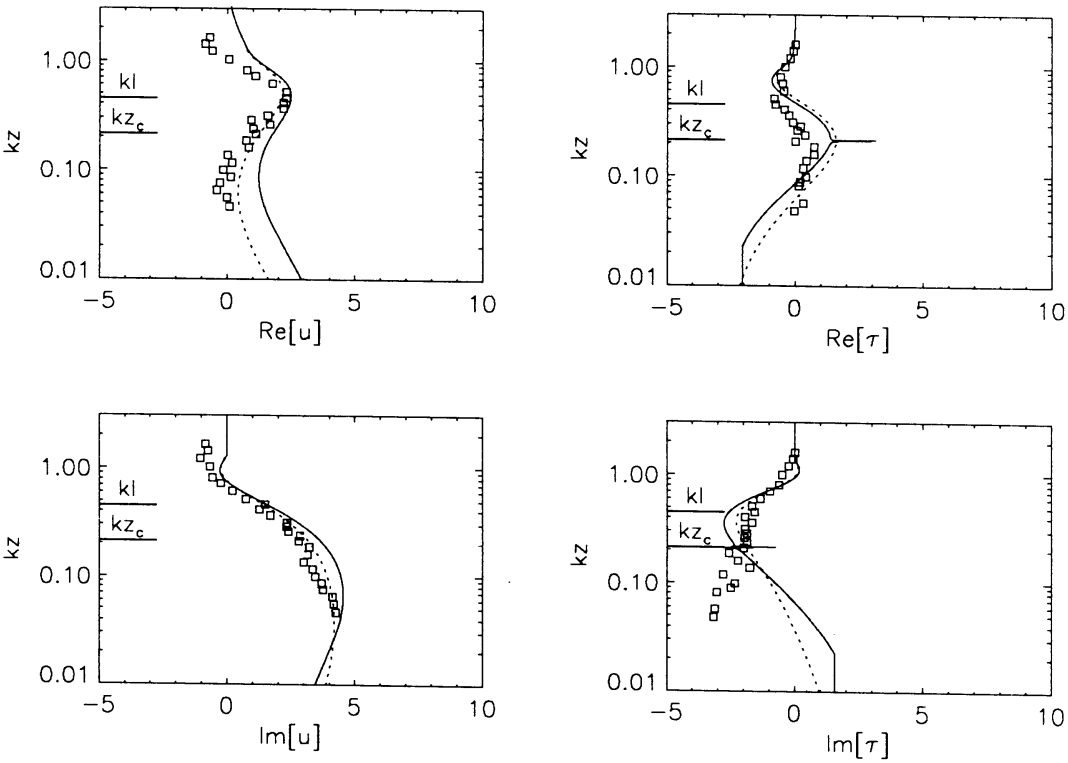

Figure 4b

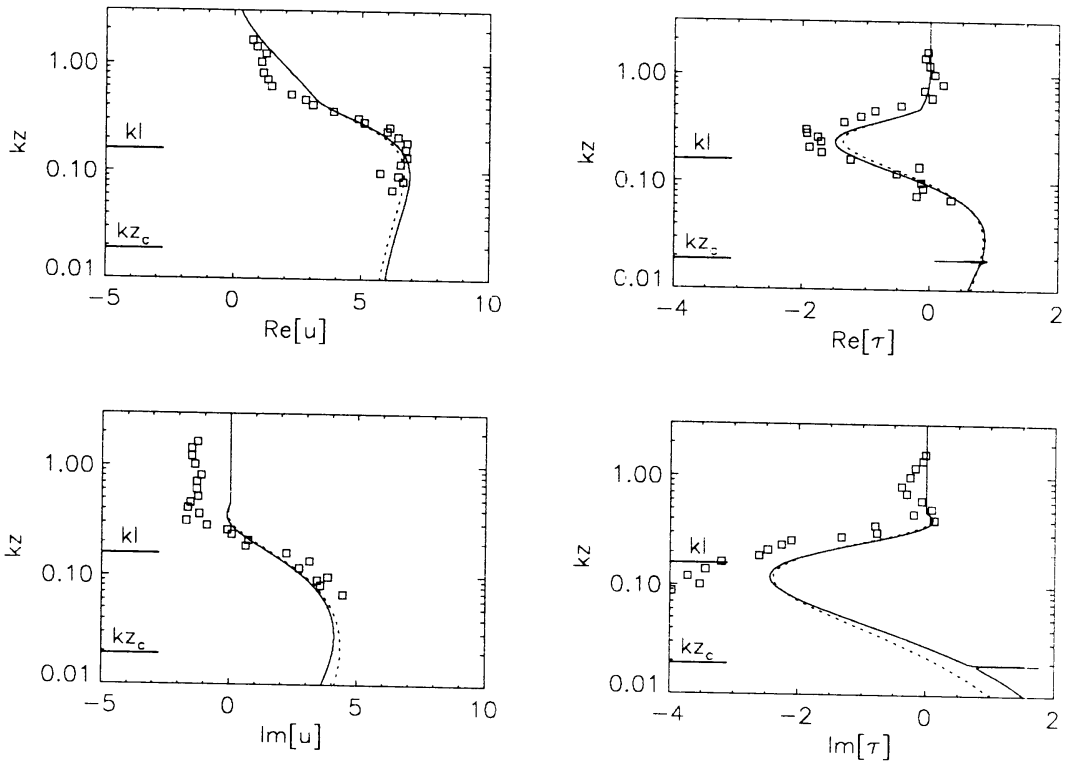

Figure 4c

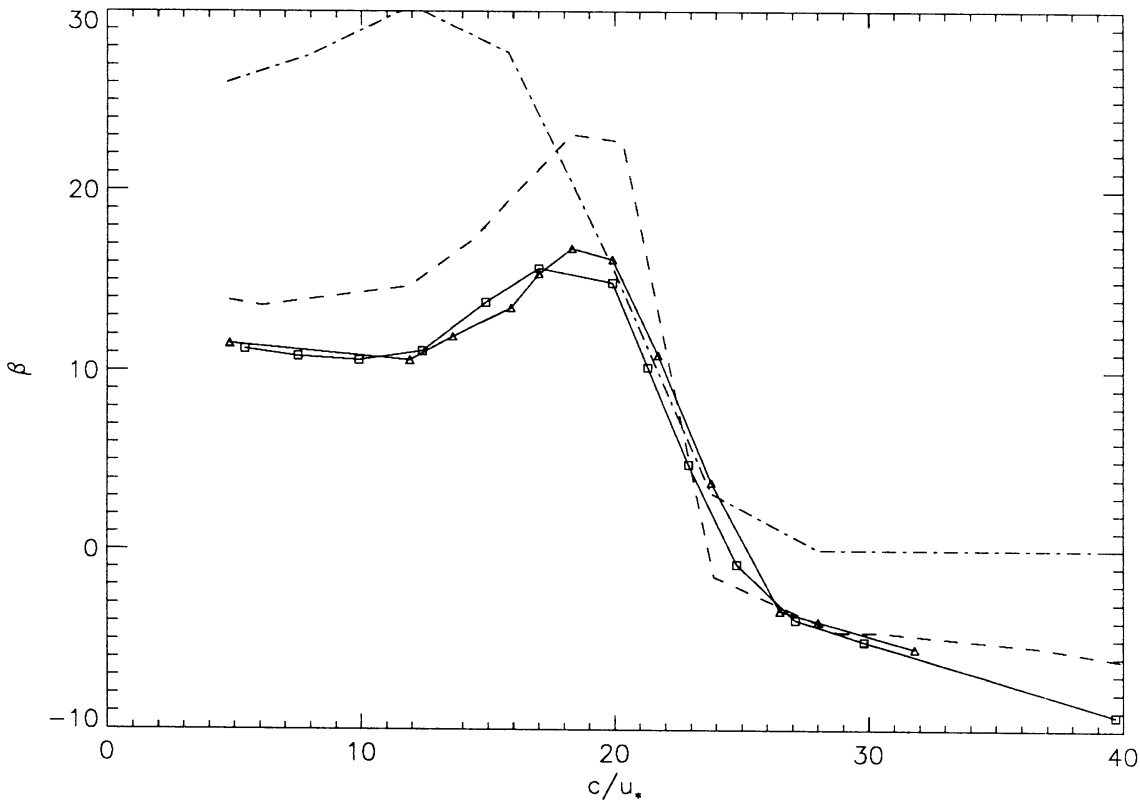

Figure 5

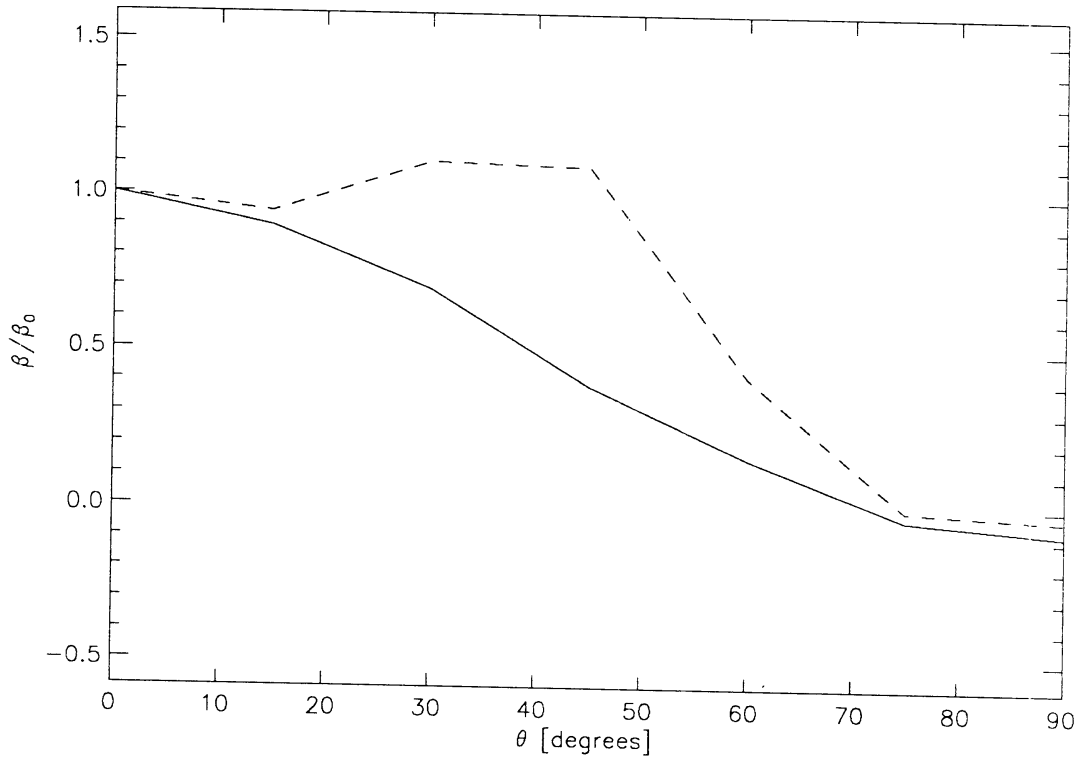

Figure 6a

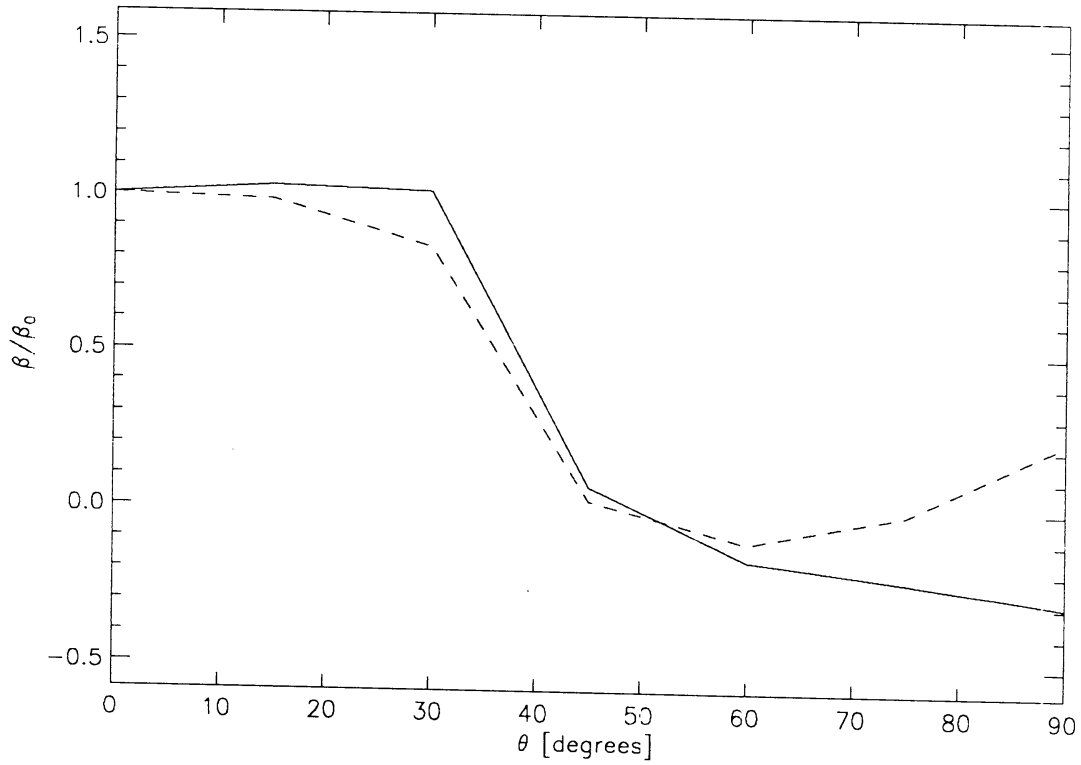

Figure 6b